Automatic Glaucoma Detection using Retinal Fundus Images

By

Muhammad Abdullah

NUST201362720MSEECS60013F

Supervisor

Dr. Muhammad Moazam Fraz

A thesis submitted in partial fulfillment of the requirements for the degree of

Masters of Science in Information Technology (MS IT)

In

School of Electrical Engineering and Computer Science,

National University of Sciences and Technology (NUST),

Islamabad, Pakistan.

(May 2016)

Approval

It is certified that the contents and form of the thesis entitled **"Automated Detection of Glaucoma in Retinal Images"** submitted by **Muhammad Abdullah** has been found satisfactory for the requirement of the degree.

Advisor: **Dr. Muhammad Moazam Fraz**

Signature: _____

Date: _____

Committee Member 1: **Dr. Anis ur Rahman**

Signature: _____

Date: _____

Committee Member 2: **Dr.Asad Anwar Butt**

Signature: _____

Date: _____

Committee Member 3: **Dr. Omar Arif**

Signature: _____

Date: _____

Dedication

To my Loving Parents.

Certificate of Originality

I hereby declare that this submission is my own work and to the best of my knowledge it contains no materials previously published or written by another person, nor material which to a substantial extent has been accepted for the award of any degree or diploma at NUST SEECS or at any other educational institute, except where due acknowledgement has been made in the thesis. Any contribution made to the research by others, with whom I have worked at NUST SEECS or elsewhere, is explicitly acknowledged in the thesis.

I also declare that the intellectual content of this thesis is the product of my own work, except for the assistance from others in the project's design and conception or in style, presentation and linguistics which has been acknowledged.

Author Name: **Muhammad Abdullah**

Signature: _____

Acknowledgment

First and foremost, I would like to thank Allah Almighty for blessing me with the opportunity to study at NUST. His continuous mercy gave me strength, motivation, and determination for doing my thesis and completing my MS degree.

I have been very fortunate to have Dr. Muhammad Moazam Fraz as my supervisor. I am deeply grateful for his support throughout my research work. In addition to being the best supervisor, he has a great passion for research. His sincere efforts, support, and guidance through the whole journey bought my thesis to light. His dedication for his work has a great impact on his students including me. I truly appreciate all his efforts specially the countless hours in enhancing my presentation skills, reading, reflecting, encouraging and most of all patience throughout the whole thesis phase.

Publications Emerged from This Research

i. **Application of grow cut algorithm for localization and extraction of optic disc in retinal images**. Published in 2015, 12th International Conference on High-capacity Optical Networks and Enabling/Emerging Technologies (HONET).

Available from:

http://ieeexplore.ieee.org/xpl/articleDetails.jsp?arnumber=7395436

DOI: 10.1109/HONET.2015.7395436

ii. **Localization and segmentation of optic disc in retinal images using circular Hough transform and grow-cut algorithm.** Published in multidisciplinary journal PeerJ which has an impact factor of 2.112.

Available from https://peerj.com/articles/2003/

DOI: 10.7717/peerj.2003

ABSTRACT

Glaucoma is among one of the top two eye-related diseases which results in blindness. This disease lacks early symptoms and as a result of that the patients of glaucoma remain unaware about the disease until it enters the advanced stage. The diagnosis of glaucoma is usually done manually from the 2D fundus images and the decision about the glaucoma presence is made on the basis of the cup to disc ratio which is derived from the size of the optic cup and optic disc. This project aimed towards the development of automatic glaucoma diagnosis system by the use of image processing techniques and machine learning approaches. The ultimate goal of the project is to drive state of the art approach for accurate glaucoma detection which can facilitate the general population for glaucoma screening. The early detection, would contribute towards the reduction of blindness cases in the world. This project is based on software which is easy to use and require fundus image as an input and the result is the detection of glaucoma even at its earlier stages. The project is divided into different modules to make it extensible for the diagnosis of other retinal diseases such as diabetic retinopathy, and macular edema. For the extraction of the optic disc, image processing techniques are used which produce good quality segmentation results while for the extraction of optic cup supervised learning approach is used in which multiclass based bagging method of ensemble classifier is used for training and classification. The results of the classifier are refined by the image processing techniques to achieve the best fitting of the cup elliptical boundary. The proposed method is tested on publically available image databases and evaluated against previous methods presented in the literature. The methods achieved much better accuracy in segmenting optic cup and optic cup and in the detection of glaucoma.

Table of Contents

List of Figures

List of Tables

Chapter 1

Introduction

1.1 Background

Glaucoma is a disease related to eye disorders that damage the optic nerve, the structure which carries visual information from retina to the brain, and cause peripheral vision loss which if remains untreated leads to permanent blindness. It is multifactorial but often occurs because of the presence of increased intraocular pressure (IOP) inside the eye but that not always be the case, as some people can develop glaucoma with normal IOP. Glaucoma is a neurodegenerative disease because optic nerve is a part of the human central nervous system and it shares certain features such as age and family history with other degenerative brain diseases like Alzheimer and Parkinson's disease. The only difference with another degenerative disease is the specific brain area that it affects, eye and optic nerve.

Indeed optic nerve and retina are part of the brain as at the time of development part of brain extend and become optic nerve to capture visual information. Inside the eye, ganglion cells collect all information from the optic nerve and pass it down to receiver end, the axon. At the initial phase of glaucoma, these ganglion cells get the damage.

The optic nerve is the always remain the main focus for researchers to determine the causes of glaucoma. Injury of optic nerve axon cause changes in ganglion cells which ultimately leads to cell death and this eventually becomes the reason of peripheral vision loss.
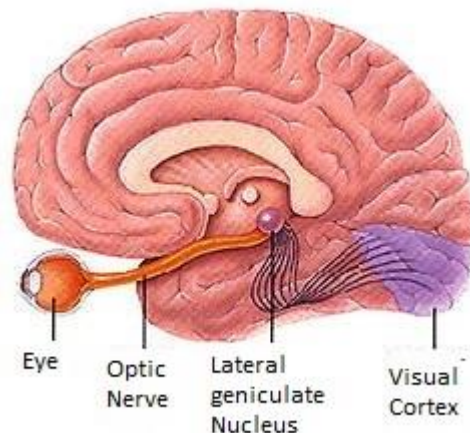
Figure 1-1 Optic nerve connection to the brain [1]

Glaucoma is the second leading cause of irreversible blindness around the world. At the current time there are about 70 million people around the world who are affected by glaucoma and this number is estimated to rise above 80 million by 2020. Glaucoma is called "silent theft of sight" because it does not show early symptoms and that is why half of the affected people don't even know about their condition. Early treatment can halt the progress of glaucoma but if it remains untreated it can't be cured because neurons, once damaged, are unable to regenerate again. Glaucoma is more likely to affect people who are above 40. In America alone, more than 3 million people are affected by glaucoma, 2.7 million of which are above age 40. Approximately 0.12 million people get blindness because of glaucoma, which accounts for 10% of all blindness cases in the US. Figure 1-2 shows the percentage of various diseases contributing People who have a genetic history of glaucoma, migraine, diabetes, blood pressure, the eye in global blindness.

People who have a genetic history of glaucoma, migraine, diabetes, blood pressure, eye injuries, and the history of steroid usage are at higher risk of developing glaucoma. Furthermore, age factor also contribute to the glaucoma progression. Multifactorial nature of glaucoma and absence of early symptoms is the reason of an increase in a

number of glaucoma cases every year. Figure 1-3 shows the rapid increase of registered glaucoma cases in the Hispanic population.
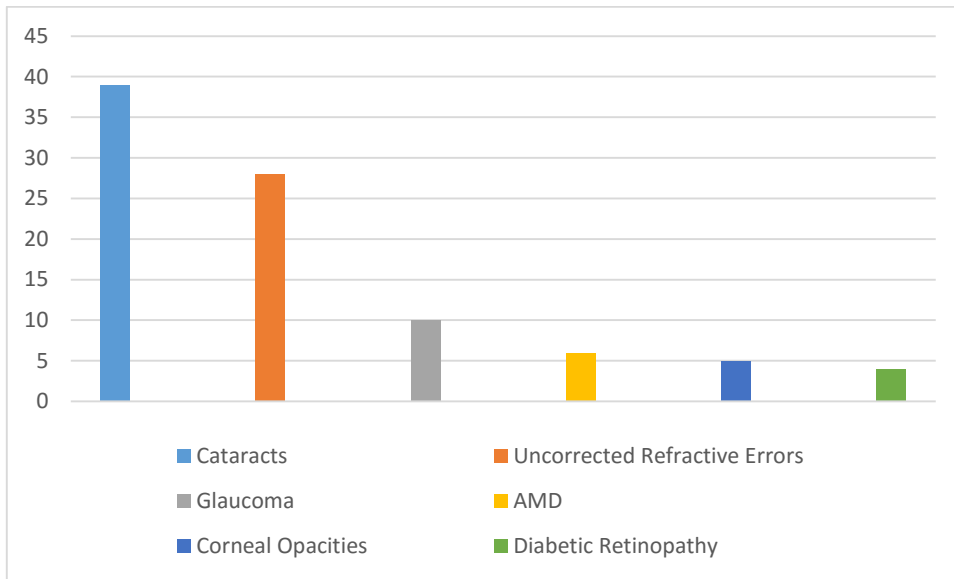
Figure 1-2 Global causes of blindness (%)
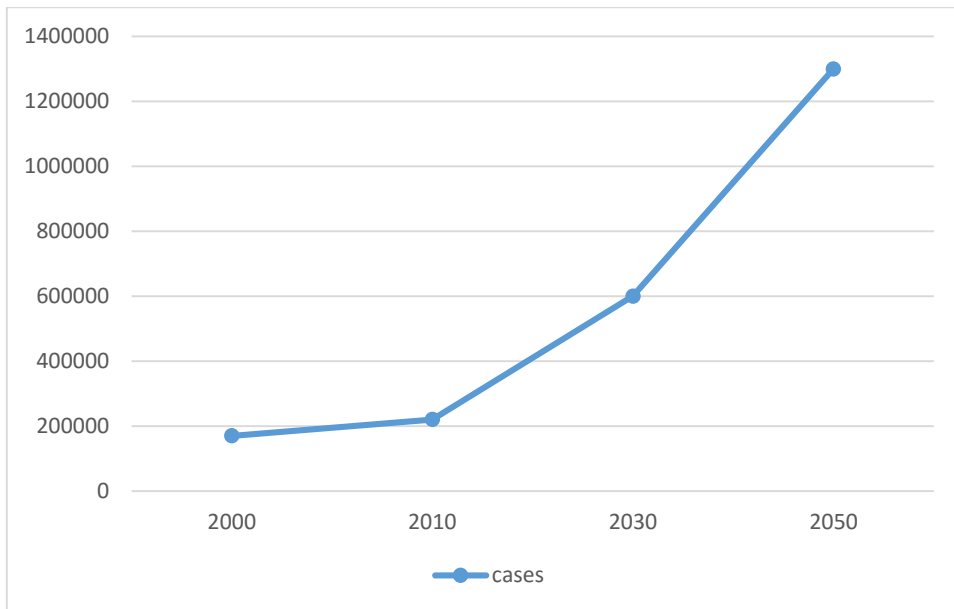
Figure 1-3 Glaucoma cases among Hispanics: Past and projected

1.2 Problem Statement

Glaucoma is the second leading cause of blindness around the world and half of the patients who are affected by this disease don not have any idea about this because it

does not show early symptoms. Symptoms appear at the advanced stage of this disease but at that stage disease cannot be cured. Hence, early detection is the key to halting the progression of this disease.

1.3 Problem Addressed

Glaucoma is manually detected by an ophthalmologist from the fundus images which make it time-consuming and limited to the hospitals, furthermore, for mass screening program it is impossible to manually analyze each image and make predictions. Our research work provides a low cast, fast and robust solution to address this problem. This automatic detection system leads to the mass screening of population for early detection of glaucoma.

1.4 Features of Solution

This software is able to detect glaucoma by automatic extracting optic disc and optic cup and calculating cup to disc ratio and making use of ISNT rule for glaucoma detection. This software can make detections on images taken from the portable lens on smartphones.

1.5 Anatomy of Eye

Vision is one of the most important sense among the five primary senses and contributes more than 75% of all information we get from the environment. The human eye is the most complex structure of the body which is about one inch in diameter. Bones, muscles, fats, and nervous system are involved in the functioning of the eye. Orbital bones and fat pads provide protection to the eye, extraocular muscles control the eye movement and optic nerve carries nerve signals to transfer visual information to the brain for processing. Figure 1-4 shows the retinal fundus image of human eye presenting different retinal structures. Cornea and sclera make the outermost layer, the sclera is outer white coat while cornea is transparent dome structure that provides optical power to the eye and covers iris and pupil. Iris makes the middle layer of the eye made up of

pigmented tissues that provide color to the eye and also involves in controlling the amount of light entering the eye by changing the size of the papillary opening, pupil. So in low intensity of light pupil dilates to allow more amount of light to pass and opposite happens in the presence of brightness. After passing through iris light enters optic lens which focuses the light to the back of the eye where the retina is located.

The retina is the innermost light-sensitive layer which covers more than 65% of eye's interior area and serves the same function as the film in the camera. When incoming light make contact with photosensitive cells, rods, and cones, of retina it triggers a cascade of electrochemical events which ultimately transforms light energy into nerve signals. These nerve signals then carry all visual information to the brain through the optic nerve. Rods and cones in the retina get excited by the neural system and generate an image of incident light. Cones are sensitive to bright light and during the daylight they facilitate the generation of a high-resolution image which is called photopic vision. The rods are sensitive to dim light and at night under low illumination, they mediate low-resolution visualization which is called scotopic vision. They are concentrated at the peripheral region and their density keep on reducing towards the center of the retina. Hence, they mediate peripheral vision and also detect motion in the dark. Within retina, there is a central small area called macula which possesses the highest density of cones nerve cells and is involved in central vision. Only a few cones cells reside outside macula, therefore, cones are mostly involved sharp central vision, which helps to get visual details.
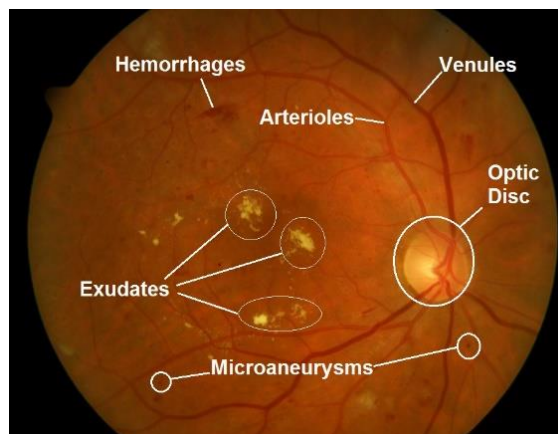
Figure 1-4 Digital fundus image of retina [2]

Rods and cones, with the help of intermediate retinal ganglion cells, pass the visual information to the optic nerve. Optic nerve open in the retina at a point called optic disc and at this point blood vessels leaves and enter to the retina. In optic disc, optic nerve has nerve fibers which are called axons receive nerve signals from retinal ganglion cells. All the visual information is passed through the optic nerve to the brain where brain cells receive the data process it and take actions on the basis of processing.

1.6 Glaucoma Overview

Glaucoma is a disease which damages optic nerve and results in vision loss. The optic nerve is the part of nervous systems so any damage to it is completely irreversible and the only solution is early detection to stop any further damage. Increased intraocular pressure may damage optic nerve but that may not always be the case of glaucoma as it can develop even under normal pressure. So measuring damage of optic nerve is now becoming a new glaucoma diagnosis norm. The major structures of the eye that directly or circuitously contribute in glaucoma progression are aqueous humor, optic disc, and optic cup.

1.6.1 Aqueous Humour

It is the watery fluid that is secreted from ciliary body and is maintained between the cornea and optic lens. Crystalline lens and cornea do not have their own blood supply so this fluid acts as a replacement by providing nutrition and keeping the eye inflated. The standard volume of this fluid is about 0.2 ml which keeps on replacing itself every other hour.

Figure 1-5 shows the pathway of this fluid which flows from lens to anterior chamber from where it leaves the eye through the trabecular meshwork and uveoscleral pathway. Any abnormality in the discharge of this fluid raises the amount of this fluid which results in high intraocular pressure. If unchecked, this high pressure may damage optic nerve and end with the onset of glaucoma. That is why this fluid is of primary focus for research on glaucoma progression.
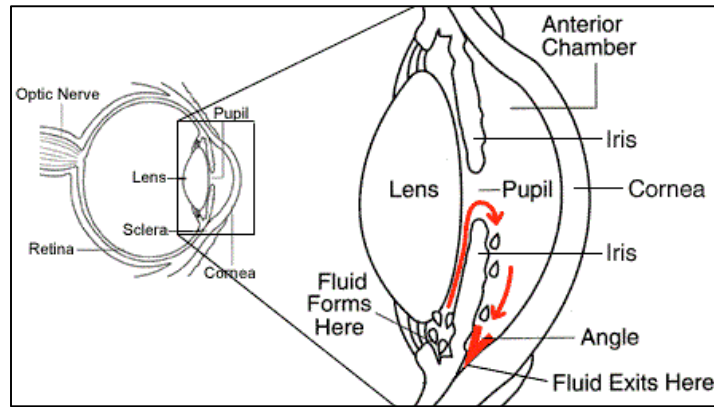
Figure 1-5 Aqueous Humour pathway [3]

1.6.1.1 Trabecular meshwork pathway

This area of tissue is porous and spongy which is located at the base of the cornea. This pathway is called conventional pathway as it is responsible for 85 percent of aqueous outflow. The trabecular meshwork consists of three parts; inner-uveal meshwork which is bordering the anterior chamber, corneoscleral meshwork is the superficial portion containing thin perforated sheets and juxtacanalicular tissue which lies closure to Schulman's canal. Schulman's canal consists of a set of tubes which are connected to blood vessels and carry the aqueous fluid to the blood stream. The outflow of fluid from this pathway is mediated by two external forces: one is the alteration in extracellular matrix cells that surround meshwork and other is the alteration within meshwork cells and Schulman's canal which induce cellular contraction.

1.6.1.2 Uveoscleral Pathway

Drainage of fluid is different in this pathway as there is no proper tubular channel to pass through, instead fluid seep through and between tissues. This pathway corresponds to the very small amount of fluid that leaves the eye and because of the absence of any well-defined structural nature, this pathway is also referred as an unconventional pathway. The aqueous outflow through this pathway is mediated by a pressure gradient which is generated as by the ciliary muscle movement or changes in the extracellular

matrix that surround drainage tissues. Figure 1-6 shows both conventional and nonconventional pathways.
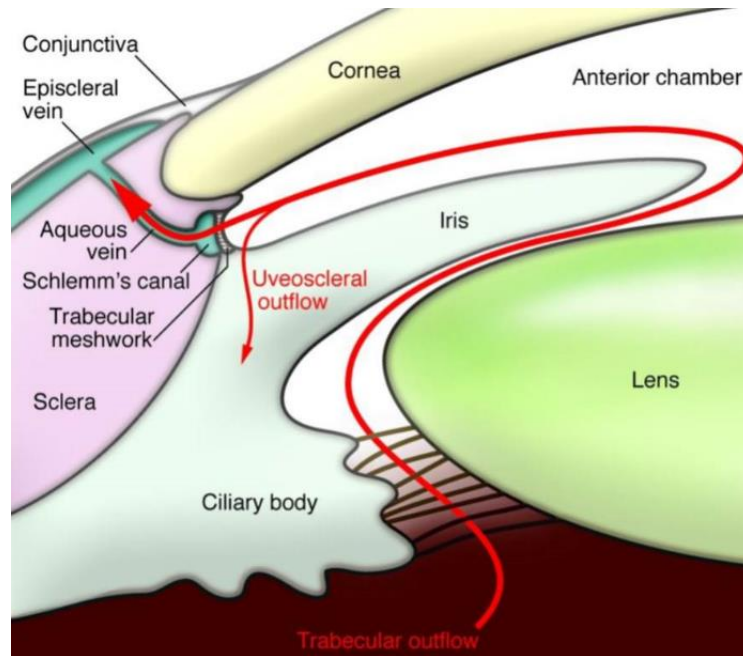
Figure 1-6 Trabecular and Uvescleral Pathway [4]

1.6.2 Optic Disc

The optic disc is the term that refers to the portion of the optic nerve that is visible for clinical examination and evaluation. The optic nerve, about 50 mm long cylindrical 3d structure that lies between the retina and optic chiasm, consists of four parts. Figure 1-7 shows the localization of four different parts of optic nerve: Intraocular which refers to the front end of retina also called optic nerve head (ONH), Intraorbital which extends from globe to optic canal, Intracanalicular which lies inside optic canal, and Intracranial which extends from optic canal and leads to optic chiasm.

The distal portion of the optic nerve, called optic nerve head or optic disc, extends just behind sclera to the surface of the retina. It is slightly oval in shape with 9% greater vertical diameter than horizontal. The optic disc is the most important structure of the eye because of its functional contribution in eye functioning and structure variation in the presence of diseases. For the purpose of glaucoma assessment, optic disc shows

several characteristics which are precious for glaucoma detection. For the evaluation of optic disc contour, color and cup are the important characteristics to measure.
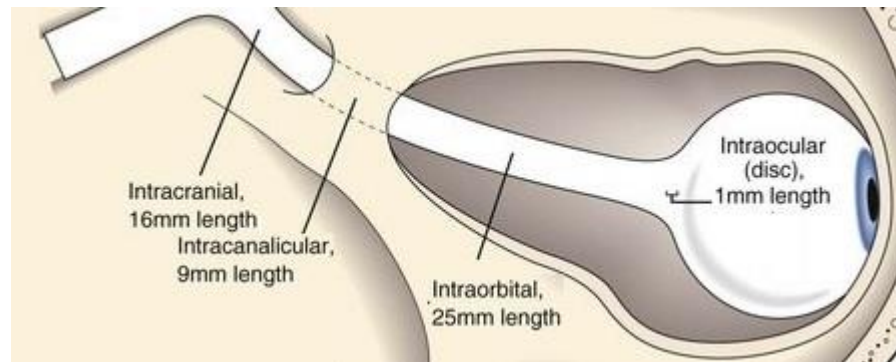
Figure 1-7 Parts of Optic nerve [5]

1.6.2.1 Disc Contour

The boundary of the optic disc should be well defined and clear in all aspects. The unclear boundary may indicate the presence of some other pathologies e.g. presence of optic disc drusen cause blurriness in of disc boundary similarly presence of papilledema cause swelling of the disc.

1.6.2.2 Disc Color

The optic disc is usually orange-pink with a light center but the presence of some other diseases may affect the color e.g. the presence of pathologies changes the color from orange-pink to pale, optic atrophy. Optic atrophy is not a disease by itself but it indicates the presence of another disease e.g. Glaucoma, optic neuropathy, and optic neuritis.

1.6.2.3 Optic Cup

Optic cup is present at the center of the optic disc and because of the absence of any neuroretinal tissue, it appears as a pale center. Usually, the vertical size of the cup is one-third of optic disc which means if the cup size is greater than 0.3 then it's the indication of glaucoma presence.

1.7 Types of Glaucoma

Glaucoma is a general term related to eye with damaged optic nerve. Primarily glaucoma is divided into two categories open angle and closed-angle, other types are normal-tension, congenital and secondary glaucoma.

1.7.1 Open-angle glaucoma

Primary open angle glaucoma, also called chronic glaucoma, is the most common type of glaucoma which accounts for 90% of total glaucoma cases. This type progress slowly, completely painless and results in gradual loss of vision which is irreversible. In this type trabecular meshwork, which is responsible for drainage of aqueous humor, gradually lost its function and results in clogging of canals which cause an increase in intraocular pressure. The high pressure damages fibrous structure of optic nerve, called axon, which conveys visual information to the brain.

Open-angle glaucoma remains unnoticeable at an early stage because there is no clear symptoms and vision is not much affected. As the damage progress, blank spots began to appear in the field of vision and with the passage of time these spots become larger and peripheral vision (corner area) is lost. Complete blindness occurs with the death of all nerve fibers.

High pressure is usually not the cause for half of the glaucoma cases. Furthermore, IOP keeps on changing from time to time so high pressure may not always be a case of glaucoma.

1.7.2 Normal tension glaucoma

Normal IOP is less than 21 mmHg, but this can lead to the wrong detection. As the people affected by normal –tension or low-tension have normal pressure but still got damage optic nerve and vision loss. This type is just the same as open-angle but is without IOP and receives the same treatment.

1.7.3 Closed-angle glaucoma

In this type iris comes close to drainage angle, thus ends up in blocking drainage angle. IOP keep on increasing as iris completely blocks drainage angle. This type is very chronic and is responsible for half of the glaucoma cases worldwide. Sudden increase in pressure is an emergency situation called an acute attack. Genetically susceptible people became the victim of this type, especially the Asian people have a high probability of developing this type of glaucoma.

An acute attack of this type is a medical emergency which must be addressed immediately but people at risk don't have any noticeable symptoms before the attack. The symptoms of acute attack are blurry vision, headache, vomit, nausea, eye pain and appearance of halos.

1.7.4 Congenital glaucoma

This is the rare type of glaucoma which affects infants at an early age and it can be inherited. In this type drainage canals fail to develop in infants. This type although have low frequency, 1 in 10,000, but it can be devastating resulting in blindness if untreated at an early stage. This condition can be cured with microsurgery.
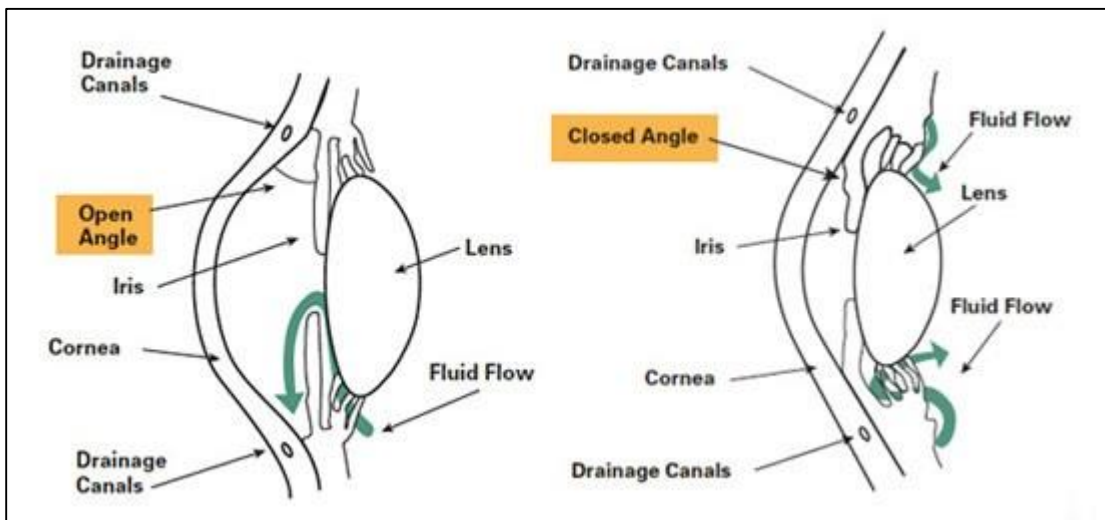
Figure 1-8 Open Angle and Closed Angle Glaucoma [6]

1.7.5 Secondary glaucoma

This type develops because of the presence of other eye diseases. People with eye injury or long term steroids history have the chance of developing this type. Pseudoexfoliative, neovascular and pigmentary glaucoma are the most common type secondary glaucoma.

1.8 Glaucoma Risk Factors

The presence of some factors can increase the risk of glaucoma development or facilitate the further progression. These factors are age, race, family history, eye related risks, corticosteroids, and another dietary intake.

1.8.1 Dietary

There is no evidence of any dietary deficiency related to glaucoma development but caffeine have been reported to increase intraocular pressure in glaucoma patients but does not affect healthy individuals.

1.8.2 Age

Age is an important factor in relation to glaucoma development as with each year of age chances of glaucoma also increase. People over age 60 are at higher risk of development of glaucoma, however, African American are influenced more by age factor and are at high risk over age 40.

1.8.3 Ethnicity and Race

In comparison to Caucasians, African Americans are at five times higher risk of glaucoma development and four times of getting blindness caused by glaucoma. In African American population, the chance of getting this disease is also high at an early age and they have 15 times more chance at the age between 45 to 60 years. People from Native Alaskans and Asian descents are more likely to develop closed-angle glaucoma and people of Japan descents have a higher chance of normal tension glaucoma.

1.8.4 Family History

Glaucoma is also related to genetics and that's why it runs in families where someone among ancestors has glaucoma history. Siblings of the patients with open angle glaucoma are at five times higher risk of glaucoma development. Previous studies show that among families which have glaucoma history may develop glaucoma at much faster pace and in most cases when patients get diagnosed they already lost some vision.

1.8.5 Medical Conditions

Previous researches indicate that high blood pressure, diabetes, heart disease, and migraine may have a higher risk of developing glaucoma.

1.8.6 Corticosteroids

Use of corticosteroid for a long time can increase the risk of developing secondary glaucoma.

1.8.7 Eye-related Factors

Several eye abnormal structures such as thinning of cornea and sensitivity of optic nerve noticeably increase the risk of getting glaucoma. Some other eye conditions such as eye tumor, a detachment of the retina and the inflammatory eye can prompt the glaucoma onset. Some researches indicate the increase of nearsightedness as a risk factor.

1.8.8 Increased Intraocular Pressure

The increase of intraocular pressure may act as a risk factor for glaucoma development. Several eye trauma or accident e.g. lens dislocation and cornea detachment may increase the intraocular pressure which may lead to glaucoma development but in some cases, higher intraocular pressure may not always be the case of glaucoma development.

1.9 Characteristics of Glaucoma

Even in the normal population, the appearance of the optic disc is hugely diverse as it may vary in size shape and color from individual to individual. At an early stage of glaucoma, changes in disc structure are very much elusive and that make it difficult to distinguish from healthy one. For the evaluation of disc specific change in patterns provide a reliable proof.

1.9.1 Neuroretinal Rim

The disc area that contains nerve fiber axons is denoted as the neuroretinal rim and because axons get damaged by the presence of glaucoma so any mutation in its structure is the key to identifying glaucoma development. For the assessment of glaucoma rim, thickness and area of that thinning are key features.

To distinguish disc damage as pathological or physiological, the cross section of the optic disc is used to detect thinness of rim in each section. This cross section is known as ISNT rule which refers to inferior, superior, nasal, and temporal zones. A healthy disc has thickest rim portion in the inferior zone, second most thick is superior then nasal and the temporal is the thinnest zone. For glaucoma evaluation thinness of temporal zone is the most important feature to measure but this may not always be true as for some cases healthy disc can break this rule, likewise, some glaucomatous disc may follow this rule.

1.9.2 Focal Notching

It is the major characteristic of the glaucomatous disc that can be apt to inferio-temporal or superior-temporal in nature. In the extreme case of the full notch, the rim may completely disappear and results in an increase of this area. It can be linked with peripapillary atrophy and can go further deep. The presence of notches directly influences vision capability.

1.9.3 Retinal Nerve Fiber Layer Defects

Retinal nerve fiber loss is relatively difficult to analyze and is not good enough for glaucoma screening but it can be useful for early detection of glaucoma or to measure ocular hypertension.

1.9.4 Peripapillary Atrophy

This feature can be related with the usual aging process but it can be associated with glaucoma. The degree of atrophy is directly related to severity and progression of glaucoma. In normal individual, this atrophy may not be permanent but for glaucoma patients, this atrophy lies in the rim loss area.

1.9.5 Optic Cup Size

The damage of optic nerve is also one of the most important key feature indicating the presence of glaucoma. Any damage to optic nerve head influences the size of the optic cup. The increase in the size of the optic cup is measured by the ratio of the area surrounded by the cup to the area occupied by the optic disc. This area is the key indicator of glaucoma presence.

| (a) | (b) | (c) |
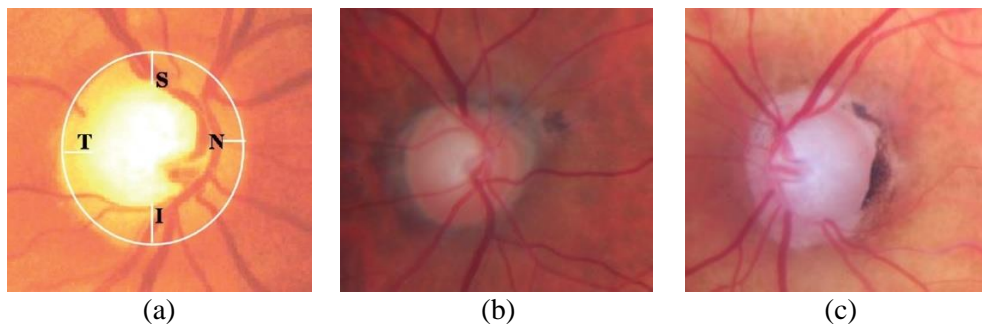
Figure 1-9 Features of glaucoma: (a) ISNT zones of neuroretinal rim (b) Focal notching of rim (c) Peripapillary atrophy [7]

1.10 Diagnosis

Measuring intraocular pressure within the eye is not enough for screening glaucoma cases as high pressure may not always be the case of glaucoma. Glaucoma detection can

only be confirmed when optic nerve damage is present. But for the case of glaucoma especially, the open angle glaucoma do not show any early symptoms as a result of which disease progress slowly without getting notice. Half of the patients don't even realize that they have the disease until the peripheral vision is lost but when it happens a lot of damage has already been done to the optic nerve and that damage is completely irreversible. So for screening glaucoma, it is important to go for eye checkup once in a while as age grows. The recommendation for glaucoma check up is once in every four years before age 40, once in every three years between ages 40-54, once in every two years between age 55-64, and once in six month period after age 65.

1.10.1 Visual acuity test

This is the simplest test that measures the sight of the patient by making an individual read text at a specified distance of approximately 20 feet. The test measurement may involve a test of each eye separately with or without lenses.

1.10.2 Tonometry

Measuring eye pressure is a primary step of glaucoma screening because high pressure may be associated with glaucoma. Tonometry is a procedure that involves measurement of intraocular pressure of aqueous humor. The procedure involves placing anesthetic drops in the eye then the plastic prism of tonometer is gently placed over the cornea to get the resistance offered by the cornea. The whole process is completely painless and can be done in a quick session. For measuring eye pressure several methods are in clinical use.

Applanation method involves the use of small force to applanate or flatten the cornea. The amount of exerted force is then used to measure the eye pressure. Goldmann tonometry is a type of applanation method and is also the most acceptable method. In this method, a prism on the head of the tonometer makes the contact with the cornea and blue light filter to measure the exerted pressure. Perkins tonometer is also another type of applanation method used for patients who can't sit for the examination.

Dynamic contour is another type of tonometry but unlike applanation, this method does not deform cornea, therefore, it's not get influenced by the thickness of the cornea. In this method, the center of tonometer tip contains pressure sensor which is placed in the center of the cornea. The electrical resistance of cornea change when the pressure of sensor is subjected to change. The tonometer measures the change in pressure in accordance with the change in resistance.

Electronic indentation method uses floating transducer which is covered by an external ring that flattens the cornea. The purpose of this method is to minimize the influence of corneal thickness.

Rebound tonometric method uses small magnetized metal probe which is fired against the cornea. The probe hit the cornea and bounce back to the device where induction coils are present. This magnetized probe induces current in coils which are used to measure pressure.

Pneumatonometry method measures pressure by using the pneumatic sensor. In this method, fenestrated membrane is placed on the surface of the cornea and pumped air in the piston of machine move through the membrane. The resistance offered by cornea alter the movement of the piston which is then used to measure intraocular pressure.

Impression tonometry method uses tiny plungers. These plungers are of known weight and are used to indent cornea. The depth offered by the weight of these plungers is used to measure pressure. When intraocular pressure is high then more weight is required to produce an indent.

Air puffed method do not involve any contact with the cornea rather it make use of an air pulse to flatten the cornea. Electro-optical system detects corneal flattening while the exerted force of air pulse is used to measure the pressure.

The normal range of IOP is between 10 to 21 mmHg. Any increase of pressure above this range raise a serious concern but for individuals with normal tension, glaucoma can still develop the disease when pressure is within specified range. Previous studies indicate that only 10 percent people develop glaucoma when their IOP is between 21 to 30 mmHg and people who have high IOP may have normal pressure for part of their life.

Researches show that factors such as corneal thickness and body posture while taking IOP test may influence the detection of accurate pressure. As compared to invasive methods, noninvasive methods are less influenced by the corneal thickness. Similarly, body posture while laying down or while sitting reflects fluctuations in IOP.

Figure 1-10 Tonometer [8]

1.10.3 Perimetry

Perimetry refers to the visual field test that is used to detect any abnormality in the central and peripheral region. Any dysfunction in visual field can be the result of any medical condition such as heart attack, glaucoma, or brain tumor. But the peripheral vision loss is associated with glaucoma. For testing visual field a manual procedure such as tangent screen can be used for detection of dysfunction in visual field but when a proper automatic apparatus is used for this purpose then this is called perimeter. Test results obtained by an automatic process or perimetry are proved to be more accurate with detailed information.

In Perimetry test targets are marked on the background and detection of these targets helps in evaluating light sensitivity. Thus, it helps in mapping and quantifying the visual field at the peripheral region of visual field which facilitated glaucoma detection. Different types of perimeters are available for visual assessment and disease detection.

The tangent screen is the simplest form of perimetry in which stimulus is pins and vision testing is performed by presenting and moving different size pins against a black background.

Goldmann perimeter uses a white hollow bowl which is placed right in front of patient and light of different frequency and intensity is projected on the sphere. This

light act as a stimulus which can be moving from peripheral to the central region or it can be static and localized to one place. This type of perimetry is very helpful for glaucoma screening.

Automatic perimetry is just like Glodmann but the difference is in the computerized evaluation of visual field. In this type same type of apparatus is used and a bright light is projected on target white background which is also called white on white perimetry. The patient is given a button and he has to press it whenever he finds a stimulus light spot generated by the machine. Attached computer takes the patient input and provides a complete map of the visual field.

Figure 1-11 Goldmann Perimeter [9]

1.10.4 Gonioscopy

This test helps in detection of the angle between iris and cornea and outputs the result as an open, close, wide, or narrow-angle. This test is very helpful in the diagnosing type of glaucoma. Different type of genio-lenses is used for this purpose.

Koeppe direct geniolens involves the use of eye drops to protect any damage to the eye followed by placement of this transparent device right above cornea. The outer surface of this device provides a clear view of the angle by minimizing total internal reflection. The only problem with this apparatus is that it operates when the patient is lie down.

Glodmann indirect geniolens use internal mirrors of the device to reflect light coming from iris and cornea and project it towards the observer. The advantage of this device is that it provides orthogonal view towards observer which can be magnified with a slit lamp. The curved surface of this device do not come in direct contact with the cornea, instead, it relies on the liquid medium which is applied before operating this device. The advantage of this device is that it can operate in any body posture.
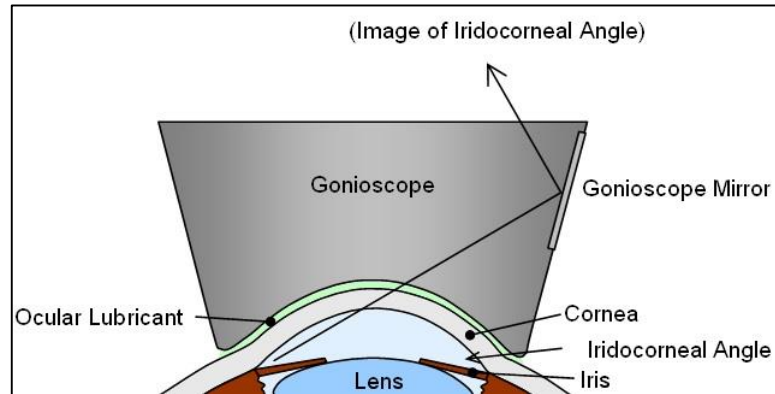
Figure 1-12 Goniescopy process to detect iridocorneal angle [10]

Zeiss indirect geniolens use the procedure just like Golsmann but the only difference is the use of prisms in situ of mirrors. It has many advantages over Goldmann as it does not require any prior lubrication and because of use of prisms it provide output iridocorneal angle in 4 different quadrants. Furthermore, the size of the apparatus is very small and it can work perfectly fine with a slit lamp.

1.10.5 Pachymetry

This test is used to detect the thickness of the cornea and has its importance due to its importance in accurate detection of IOP. Once the thickness of the cornea is known, results from tonometry can be more accurate for pressure measure. This test is very simple and painless in which probe is placed right above cornea. The probe has ultrasound transducer at it top to catch ultra-high definition echograms. Some other pachymetry processes make use of corneal waveform which can more accurately detect the thickness of the cornea.

Figure 1-13 Pachometry device [11]

1.10.6 Optic Nerve Testing

The optic nerve is the part of nervous system that collects visual information from the retina, convert it into electrical signals, and carry it to the brain for processing. The testing of damage done to the optic nerve head is an important way to test glaucoma progression. As a result of damage, optic nerve head may disappear or lost its thickness which induces changes in the size of the optic cup and changes the cup to disc ratio (CDR).

1.10.6.1 Tomography

Tomography uses laser camera to scan area around optic nerve and gets images of deeper layers of optic nerve. Its working is just like ultrasound imaging but the only difference is in the use of light rays, instead of sound, and on the basis of reflected light it generates a series of images at different depth. These images then combined to make 3d-image of optic nerve. Depth of the optic nerve changes with the progression of the disease and optic nerves keep on shrinking and thinning. So in this technique depth and width of optic cup is used to measure the glaucoma progression. There are two types of tomography used for glaucoma diagnosis: Optical coherence tomography and Heidelberg Retinal tomography. Figure 1-14 shows how optic nerve got thin in the presence of glaucoma. The limitation of tomography lies in its high cost and inability to solely diagnose glaucoma as previous studies show that evaluations from other techniques are required in order to confirm the diagnosis by this technique.
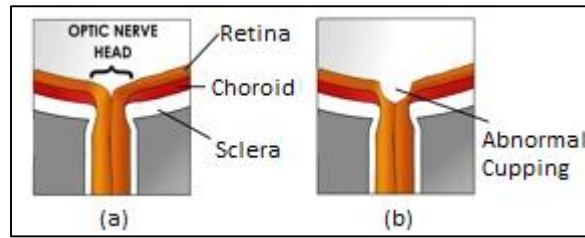
Figure 1-14 HRT images of optic nerve (a) normal optic nerve head (b) thin optic cup [7]

1.10.6.2 Ophthalmoscopy

This test is useful for the detection of the extent of damage done to the optic nerve. The preliminary step of this process involves the use of eye drops for pupil dilation, the next step is the application of device over the cornea. The device has the light at the end of the device to enlighten and magnify the optic nerve. In the presence of any abnormality in optic nerve or increase of IOP then further testing like perimetry or gonioscopy can be applied for a reliable diagnosis.
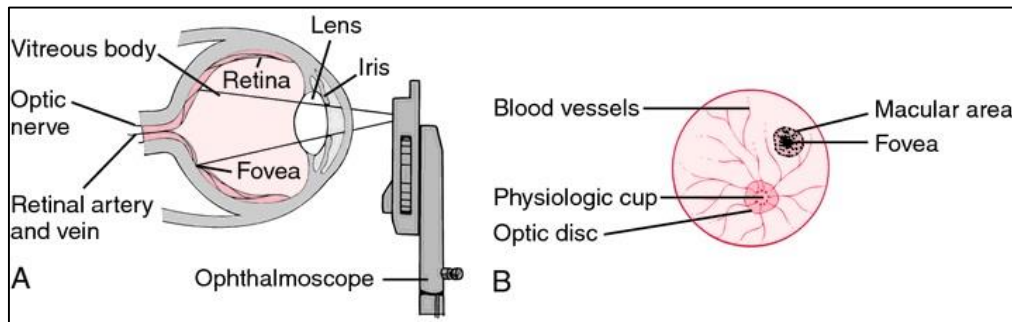
Figure 1-15 Ophthalmoscopy (A) Process of examining optic nerve (B) Structures visualized by ophthalmoscopy [12]

1.10.6.3 Fundus Photography

Fundus photography is able to not only capturing the retinal structures like fovea, macula, optic nerve head, optic disc, optic cup, and blood vessels but also other pathologies like papillary atrophy, exudates, drusens and rim notching. In the process of image capturing pupil serves a dual function by allowing illumination from fundus camera to enter retina and imaging rays to exit. The image is captured when patient put his face towards fundus camera where chin rest and forehead bar is located, next step is the focusing of the camera towards retina and this step is performed by the operator of

the fundus camera. After making initial adjustments photographer fires illuminating light beams from the camera, which create fundus photograph as shown in Figure 1-16.

A fundus camera is a smaller version of microscope which has an attached camera, the design of which is obtained from indirect ophthalmoscope. Figure 1-4 shows the structure of a typical fundus camera. The angle of view, the acceptable angle of the lens, is the main feature to quantify fundus camera. Normal angle of view is 30°, which magnifies the image 2.5 times larger. Wide angle fundus camera has an angle of view ranging from 45° -120° and that results in a small magnification of retina. The narrow angle of view is 20° or even less than that.

Figure 1-16 Fundus camera [13]

The optical design of the camera is inherited from the ophthalmoscope. The light source of the fundus camera generates light which passes through different filters to a circular mirror which reflects the light to numbers of lenses and finally the beam of light leaves the camera and illuminates the retinal structures. The illuminated retinal image is passed through the pupil and the frontal camera lens, the image formed here is a primary aerial image. This image is further focused with the help of focusing knob of the camera, by adjusting the knob, the image is focused on the back of the camera where film plane is located. Focusing knob adjusts the position of the lenses to make a clear focused image.

Focusing remove spectacle refraction or any other optical error which occur because of distance between ophthalmic lens and eye.

1.10.6.4 Advantages

Fundus photography has several advantages over other existing methods as it is cheap, easy to use and most importantly it's noninvasive. Unlike ophthalmoscopy it is much easier to use and just required basic training to handle the photography, furthermore, fundus images provide more details about the image. In ophthalmoscopy, there is does not offer any mean to store record and require manual processing as well.

With the advancement if technology, fundus images can now be captured without dilating pupil which avoids the dangers related to pupil dilation as previous studies show that dilating pupil can cause closed angle glaucoma.

The main advantage of fundus imaging is its ability to detect various eye related disorders at early stages. The diseases that cause blindness such as glaucoma, diabetic retinopathy (DR) and age-related macular degeneration (AMD) can be detected with this technique.

1.10.6.5 Challenges

Although fundus camera is easy to operate and with basic training, lab technicians can take fundus photographs but the main challenge is the interpretation of these images, a handful experience is required to analyze those images and make predictions on that. In order to handle this problem, National Healthcare Group introduced guidebook which contains all guidelines to how to interpret fundus images.

The main challenge is the presence of a huge diversity of the normal fundi among the population. Various factors such as race, myopia, age and some others directly influence the appearance of fundus images. Furthermore, the size and appearance of the optic disc is not constant and varies from individual to individual.

The presence of diseases such as glaucoma, diabetic retinopathy, and macular pucker may change the appearance of different retinal structures. For example, the presence of pathologies like exudates, papillary atrophy, rim notching, holes, tears, pigmented

lesions, masses, and detachments change the appearance of fundus image and make it difficult to analyze the presence of some disease.

Some other challenges which are not related to any medical condition but are in fact related to the image capturing are poor contrast, brightness artifacts, uneven illumination, and poorly focused images. These artifacts may blur or in the extreme case completely hide different retinal structures, thus making it difficult to make a decision on the basis of that.

1.11 Medical Image Computing (MIC)

It is an interdisciplinary field which lies at the intersection of medicine, computer science, mathematics, and data science. MIC develops mathematical models, computational methods and algorithms for solving problems related to medical images and to use them for clinical care and biomedical research. Unlike medical imaging, this field does not aim towards the image acquisition rather it focuses on the extraction of relevant information from the image and presents an analysis on the basis of acquired information. Image segmentation, physiological modeling and registration are the subcategories of this field.

In medical image analysis image segmentation is the most widely used technique to extract the required structures from the image. Segmentation process divides the image into segments which correspond to the different tissues, cells, pathologies, and other relevant structures. Unlike other segmentation processes, medical image segmentation is a pretty difficult task due to the presence of several ambiguities, pathologies, low contrast, large variation in appearance, and noise. Several image processing and computer vision techniques help in the segmentation process of the medical image.

1.11.1 Image Processing

It processes the images by taking the image as an input and process it using mathematical operations by making use of signal processing. Several image processing techniques have been developed which treat the image as a 2-D signal and process it by using signal processing techniques. Image processing is low-level processing on the

image which usually involves processing raw image, without any prior knowledge, transform it into more readable and enhanced form by using several techniques like smoothing and blurring/sharpening which involves pixel operations, contrast stretching, and edge detection which involve local operations, and image restoration. In medical image analysis, these image processing techniques are preeminent as they allow to get more details out of an image by removing noise, adjusting brightness artifacts, and hiding irrelevant information by applying morphological opening and closing operations on the image.

1.11.2 Computer Vision

Computer vision is closely related to the image processing but the only difference is that it involves high-level processing on the image to produce human-like decision on the basis of analysis and prior knowledge. To achieve this, it uses methods from image processing, machine learning, and pattern recognition. The use computer vision and image processing are based on the type of required output e.g. if the requirement is to get enhanced image with fine details then image processing is the best choice but to get a humanoid response like object recognition, automatic driving, and defect detection then computer vision is the best option. Medical image processing is one of the application area of computer vision where extracted information from the image is used for medical diagnosis. Application of computer vision in medical imaging includes image enhancement, detection of several diseases, and research work. In medical image processing, computer vision is also widely used for segmentation and in the development of computer aided diagnosis systems by using methods from machine learning and image processing.

The formation of computer vision system is dependent on type of application but usually, it follows the following order, image acquisition, preprocessing, segmentation or detection, high-level processing, and decision making. Preprocessing is the step where image processing methods are used for resampling, noise removal, contrast enhancement, and scale space representation which is used for enhancement of image structures. In feature extraction step, features like lines, edges, intersection points, blobs,

texture, shape, and color are extracted from the image. High-level processing step involves verification of data points, estimation of object size, and image recognition to classify detected object. Final step of decision making makes decision on the basis of previous steps and background knowledge. In medical image processing, this decision is usually in the form of disease detection.

Chapter 2

Related Work

The lack of automatic detection system for glaucoma diagnosis leaves the ophthalmologist to rely on clinical methods which are sometimes invasive. Manual observations from these methods is very time-consuming and therefore not a practical approach for mass screening of population. To overcome this problem different research efforts were carried out to detect features which are related to glaucoma as they can help in the diagnosis of glaucoma in noninvasive and time efficient manner. In research domain, many methods have been proposed for automatic detection of glaucoma. Most of these methods are based on segmentation methods while some others are based on non-segmentation approach, both type of approaches aim to capture features from retinal fundus images which reflect changes with the development of glaucoma. Optic nerve head is the most important structure for segmentation based methods, as the analysis of ONH helps the diagnosis of glaucoma, so extraction of ONH along with its other anatomical structures is the main important task for these methods. Non-segmentation methods focus on the detection of retinal nerve fiber layer (RNFL) defects, as RNFL lose its thickness with the progression of glaucoma, so for making diagnosis these methods do not require OD detection and segmentation. Different methods have been classified on the basis of image processing technique which they use for segmentation and are displayed in Figure 2-1, in the form of hierarchy.

2.1 ONH localization

ONH localization is the primary step towards the detection of other anatomical structures, registering changes in OD region and tracking vessel direction map. Detection of any pixel that belongs to OD region helps the process of OD boundary extraction. Based on the type of proposed methods, localization methods can be divided into three main categories.

2.1.1 Detection of OD as the brightest area

Research efforts in this category focus on calculating pixel intensity. Normally optic disc is the brightest region with high-intensity pixels, so thresholding pixels of the colored or greyscale image to a certain level helps the detection of this region [14].

Sinthanayothin et al. [15] use Intensity Hue Saturation space and perform local contrast color enhancement for the detection of the optic disc. The pixel intensity in optic disc region was enhanced by variance image, after image conversion to RGB space the optic disc region attain the highest intensity as compared to the rest of the image. They tested their proposed algorithm on a local set of database and get the highest success rate in accurate detection of OD, but other researchers found its weakness over images which have pathologies, uneven illumination, and strong vessels [16]. However, the use of image processing techniques to overcome the pathologies and other artifacts may significantly improve the success rate over a wide range of images. Walter et al. [17] proposed a method for automatic localization of OD in which they determined the threshold by selecting 2 percent of image pixels. After thresholding, OD region appears as the largest area and pixels lie in that region are treated as OD pixels. For testing of their method, they use thirty images and were able to correctly detect OD in normal images but the method lacks its strength when tested on low contrast image. Sekhar et al. [18] further extend this method to improve its performance and to achieve that they apply shade correction on images by using mathematical morphology. In mathematical morphology, the shape and form of geometrical structures, which are present in retinal images, is manipulated to perform analysis on those structures [19]. After application

of shade correction, OD appears as the largest area in the image. The application of shade correction significantly improves the accuracy in localizing OD but it does not influence on the locating the OD. For the detection of OD both methods use the Circular Hough Transformation (CHT) [20], which is the algorithm for the detection of circular objects in the image.

Although the approach to localize OD by assuming it as the brightest region appears to be pretty simple but the method is unreliable as the presence of pathologies specially lesion and exudates, which also appear as the bright region in the image and therefore may be confused with actual OD. Furthermore, the presence of brightness artifact, which is a major influencing factor in most of the retinal image, affect the intensity of pixels in the OD region and they may not appear as the highest intensity pixels in the image. This poses a straightforward contradiction to the assumption of this approach.
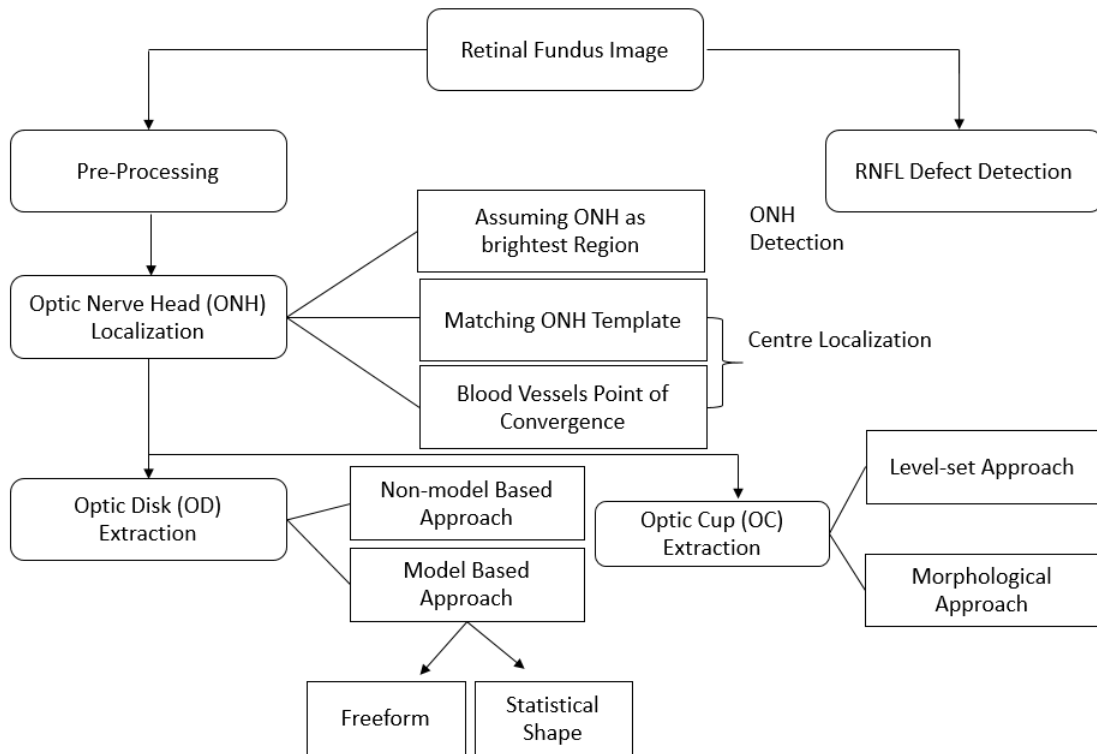
Figure 2-1 Hierarchical view of different methods based on segmentation approach.

2.1.2 OD center detection by template matching

The methods proposed in this category are based on creating an OD template and this template is used to match the OD in the test images. Although this method produces much better results as compared to the first approach but the process is time-consuming and not that much fast. In the later stage, the computational time was reduced with the maturity of this approach and the development of efficient algorithms.

Li and Chutatape [21] use Principle Component Analysis (PCA) for the modeling of OD texture. For the localization of OD in the test image, first the image was divided into sub parts and for each part, Euclidian distance, which was obtained from PCA model, was calculated. The sub-images which have OD at the center will have will have smallest Euclidian distance, OD center was located by this smallest distance. The method presents accurate results at the expense of high computational time. Although the computational time may be reduced by the image resizing as the computation is fast at low resolution because it has a small number of pixels for processing but the use of much smaller resolution may lose significant important features and thus result in inaccurate detection. So keeping a tradeoff is required between computational time and accuracy. Osareh et al. [22] perform the comparison between template image and target test image by measuring the normalized correlation coefficient. For the generation of template image, they used an average of 16 normalized fundus images. The highest normalized correlation coefficient value was used for the detection of OD but that value may not always be the exact center. For improving the performance of their method they further process the template by splitting the OD into sub-parts and the largest part was approximated to half OD. In the next step, algorithm iteratively works on error minimization between pixels in the actual and estimated arc. The OD center was approximated by the center of the circular arc. To reduce the computational time of the proposed method they incorporate a preprocessing step to minimize the algorithmic computations.

Lalonde et al. [23] used a circular template and pyramidal decomposition for the detection of OD center. They determined that at the fifth level of pyramidal

decomposition the only bright area that left in the image is OD region. At each iteration of pyramidal decomposition, the image is reduced to one fourth of original image. The brightest pixel obtained at the fifth level is used to determine OD region for edge detection of various anatomical structures. On the basis of strongest edge, this edge map was thresholded and the pixel based comparison of the circular template was made with strong edges. The purpose of this whole process was to reduce the computational time and the OD center pixel was approximated by comparing the pixel with lowest Hausdorff distance with the template. The results of this method were comparable to other methods with an advantage over computational time. The method was reported to fail for some cases of retinal pathologies were brightest pixel was located at a far distance from the actual OD center and when OD has involute blood vessels. The results of the method can be improved further by introducing preprocessing step to reduce artifacts. Youssif et al. [24] use vascular structure to determine OD center, for that purpose they use directional matched filter to capture the direction of blood vessels close to OD region. They use a nine by nine size window on test image to get the pixels belonging to vascular structure and the pixel which have the smallest accumulative distance was used as an OD center. Yu et al. [25] proposed a template based approach in which they search for OD region by using a binary template. At the next step, Pearson correlation coefficient was calculated to sort the OD region pixels and to determine the candidate pixels. Finally, standard deviation of those candidate pixels was calculated and the candidate which have the highest value of standard deviation was considered as OD center.

As compared to OD detection as the brightest region, template matching approach provides many accurate results with exact center detection even when images are affected by uneven illumination. Despite the fact that template based approach is better than the brightest region approach but still it fails and produce false detection in the presence of artifacts and pathologies. Circular arc and PCA were initial steps towards template matching and have high computation time while pyramidal decomposition based method though reduce the computation time but still couldn't overcome the failure in the presence of artifacts. Furthermore, even if blood vessels are removed then

it decreases the template quality and reduces the accuracy. The introduction of directional matched filter approach made further improvements by reducing the computational time and increasing the accuracy of determining the OD center but this method fails in the presence of retinal diseases like glaucoma which results in formation of atrophy which surrounds OD and accuracy in deterring OD center significantly reduce as this atrophy also get segmented out along with the vascular structure.

2.1.3 OD center detection by vessel convergence point

The third approach used by the researchers was to use vessels point of convergence to localize OD center as all the blood vessels in the retina converge at the OD region and exit from the retina through OD area. So the aim of applying this approach was to avoid false detection of OD region as OD is the only convergence point for these vessels. The correct segmentation of vascular structure is the main challenge for this approach, furthermore, however, if the segmentation of vessels is achieved accurately failure in deterring OD center by template matching may be overcome. Hoover and Goldbaum [26] proposed a method for the detection of vessels convergence point. After the segmentation of vascular structure they use a voting system to determine the intersection point of vessels and OD center was regarded as the highest voting point. In the next step, different regions were obtained by applying the illumination equalization and classification of OD region was performed on the basis of region size. However, the introduction of region circularity as an additional parameter may increase the accuracy of the method. Foracchia et al. [27] used a mathematical model to approximate the whole vascular structure and determined the point of convergence of vessels for the OD center detection. This algorithm have flexibility in vascular segmentation as the exact segmentation is not necessary for detection but on the downside it may fail in the low contrast OD area. Ying and Liu [28] Used fractal dimension of vascular structure which is the ratio of comparison between statistical complexities to change in detail of pattern. The fractal dimension was 1.7 within OD region which was the highest compared to other bright areas. The method was reported to apply on DRIVE database but the accuracy of the method was not provided and authors reported the failure on images

which have low resolution. Park et al. [29] Used tensor voting for the extraction of the vascular structure. As the first step, they perform contrast enhancement as the preprocessing step and then the tensor voting was applied which use geometrical features to select candidates. After segmentation of vessels, they use mean shift to find out the increasing point of density which leads to the convergence point of blood vessels. The method was reported to fail in the presence of diseases which causes lesions. Mahfouz and Fahmy [30] made use of an observation that central retinal vein extends vertically from ONH and then branched out horizontally. For OD center detection they use vertical and horizontal edge maps as the highest projection of vessel in both direction will lead to center point detection.

As compared to other two approached of OD detection, Vessel convergence point determination proved to be efficient and reliable. However, in the presence of diseases, the methods may lead to false detection as the white lesions which result from the presence of DR misguide the algorithms similarly glaucoma affected images may have PPA also causes failure. The performance of the algorithm in diseases condition is the most important as the detection of OD in glaucoma images helps in the segmentation of OD an optic cup. Thus, extraction of best features from different vessel convergence based algorithms may increase the accurate localization of OD even for the diseased images.

2.1.4 Optic Disc Extraction

The previous research efforts for OD extraction can be divided into two main categories, one is a model based while the other is the non-model based approach. In model-based segmentation OD boundary is extracted via mathematical model while different image processing techniques are used in non-model based approach.

2.1.5 Non-model Approach

Non-model-based approaches involve OD extraction by the use of image processing techniques like morphological operation and thresholding and approximation of OD as an elliptical area. The morphological operation is the first step which is followed by the

approximation step. Initially, OD was known to have a circular shape so it was approximated by circular shape but the later research reveals that it is not entirely circular and have slightly oval appearance.

Walter et al. [17] converted RGB image into Hue Luminance Saturation space and then perform thresholding for the detection of OD. After OD detection, the boundary of OD was extracted from the red channel of RGB image by applying watershed transform [31]. The red channel of the retinal image was observed to contain most information about OD boundary. Superpixels were generated from the watershed transform which divides the image into smaller regions which combine the local intensity pixels. The constraint of OD location was applied on watershed transforms to get the OD boundary but the occlusion of blood vessels in the OD region poses serious concerns on the segmentation. That problem could have been solved by the use of modern state of the art Simple Linear Iterative Clustering (SLIC) algorithm for the generation of superpixels [32]. Nayak et al. [33] took the red channel from RGB color space and use morphological operations on the image to get the boundary of OD while for the optic cup extraction they use the green channel as it retains most of the cup information. At the last step, they calculated vertical cup to disc ratio for CDR calculation. Their algorithm produces good results but the algorithm was tested on small dataset so to achieve better evaluation and generalization, a wide variety of images could better evaluate the results. Similarly, 50 used fuzzy histogram for OD boundary extraction and claimed to achieve better results than Gradient Vector Flow (GVF) model based technique but the difference in results between these two techniques was due to evaluation of former method was on very small local database of images while the later was evaluated on huge set of images with wide variety of images. In [34] they extracted OD region by correlating roughness index with the histogram.

Zhu et al. [35] applied morphological operation on luminance gray scale image to get the edge map of the image. Luminance grayscale image is the combination of normalized RGB scale. In the next step, they applied Hough Transformation on edge map to get the OD boundary but the authors pointed out the weakness of the method on images with low resolution. In [36], CHT was used for the approximation of OD

boundary but before the application of CHT they first remove the vessels from the image then they applied CHT. Although the results were promising as compared to the circular ground truths established by the ophthalmologists but the author pointed out that other elliptical approximation based methods and deformable methods may produce much better results than CHT. In [37], genetic algorithm was applied, by hypothesizing intensity level and geometrical properties, for the elliptical approximation of OD boundary. The method was evaluated on DRIONS-DB and use the difference between pixels to measure accuracy. The weak points of the method were computation inefficiency and failure of the method in the presence of PPA region. However, the performance of the method could be increased by using statistical properties like entropy but that can only solve the problem of boundary approximation in the presence of PPA region. The computational inefficiency might be reduced by resizing the image to a lower resolution so that algorithm perform operations on few pixels.

Köse et al. [38] Thresholding was applied for OD segmentation but for thresholding they use a wide range of criteria such as higher pixel intensity percentage and pixel intensity comparative to total background intensity values. The only evaluation of accuracy was based on vertical disc diameter. This method was claimed to perform OD extraction in healthy images and the images which were affected by AMD. No result was reported on the images affected by DR and glaucoma. In [39], K-mean clustering was applied on the image in YUV space. They calculated rectangular CDR and made a comparison on the basis of CDR with the established ground truths y the ophthalmologists.

In non-model based approaches extraction of optic cup and optic disc help in the calculation of vertical and horizontal CDR. CDR is the most important measure for the detection of glaucoma, although, CDR along with another measure like neuroretinal rim thickness helps the accurate detection [40]. Exact segmentation of OD is very crucial for the accurate CDR calculation, therefore, some model-based approaches were also proposed which claim to achieve good OD segmentation.

2.1.6 Freeform modeling approach

Modeling methods can be classified into two categories one is freeform modeling and the other is statistical modeling [41]. For the freeform modeling, there is no specified structure exist for the template. Active Contour Modeling (ACM) [42] approach falls into this category which involves deformation of contour according to the constraints which are specifically image based. Different energy functions, which may be external or internal, define the behavior of those contours which are based on parameters. Image features such as edges, texture, and intensity help in defining the external energy function and is used for the detection of the model region while the internal energies like rigidity or elasticity help to define modal curvature and may also aid the smoothness constrictions to avoid deformation. The modal tries to minimize its energy function and that property helps the contour to slide towards target region.

In [43, 44], they used YIO space and perform morphological operations as the preprocessing step and then applied ACM for the OD boundary extraction. In a preprocessing step, to retain the contour of the disc when removing vessels use dilation followed by erosion which avoids any damage to the disc boundary. After the removal of blood vessels in the OD region, they initialize ACM inside the OD region. The contour fitting to the disc boundary was obtained by using Gradient Vector Flow (GVF) which was obtained from edge maps [45]. The resultant boundary fitting of the contour was not dependent on the initialization point. Because of use of morphological operations, the methodology proved to be more effective as compared to the direct implication on the retinal images. However, the testing was performed on the nine images and no comparison was made for evaluation of the method. Osareh et al. [46] extend the previous work but instead using gray scale they prefer to use lab space claimed to achieve better boundary adherence of ACM as compared to the other proposed methods. Xu et al. [47] made some changes in the energy function of the contour by introducing control points vector with reference to smoothness, median intensity, and gradient orientation. For the initialization of the contour, they use CHT. Furthermore, k mean clustering was used for the grouping of contour points into two

categories: uncertain points and edge points and with the progression of the algorithm the contour points keep updating their position. By the application of process, edge points lies adjacent to the actual position while uncertain points are updated to their relevant point. The algorithm was proved to be highly accurate but in the presence of disease condition, like PPA region, algorithm failed to converge for OD boundary extraction.

Joshi et al. [48] Level set approach was used where zero level set of Lipschitz function [49] was used to define contour. Authors reported to achieve good results for extracting the OD boundary in the presence correct initializing parameters but the method was reported to be very inefficient. Yu et al. [25] further extended the work and use regional intensity information to make it computationally efficient but that proved to affect the accuracy of the previously proposed work.

As compared to the non-model based approach ACM proved to be much better in term of accuracy but again just like other methods it lacks the strength of segmenting OD in retinal images which are affected by the disease especially the glaucoma when PPA exists around OD [50]. Furthermore, the robustness of the method is another serious concern as all proposed methods were evaluated on the local image datasets. To achieve generalization these methods need to be tested on publically available databases.

2.1.7 Statistical shape modeling

Methods which fall into this category undergoes some sort of training for the detection the shape of the object. For the segmentation of OD, the methods in this category make use of ASM. ASM use a statistical model and denotes the approximation of the shape of an object. The deformation of the ASM helps in determining the shape of the boundary. This deformation process keeps the shape of the OD for the training set and takes decisions accordingly.

Li and Chutatape [51] proposed a method to model the OD boundary by using deformation of ASM. Image gradient was used to differentiate the disc edges from other images present in the image. Authors made a comparison based on Mean Distance to

Closest Point (MDCP) of their method with the ground truths obtained from different ophthalmologists. FENGSHOU [52] tried to select the best candidate points while searching for edge and to achieve that they used smallest Mahalabis distance from the mean vector. The added the gradient information to the mahalanobis distance in the form of weight. Before the application of this method, they first applied by assigning weight to color channels and then combine the image and then applied the deformable method. The evaluated their method on the basis of MDCP and another available benchmark. Roerdink et al. [31] defined the boundary on the gradient image to reduce the search space. This constraint on the search space improves the performance of the ASM. But the method can further be improved by the use of preprocessing techniques to reduce the influence of vessels in the OD region. Li et al. [53] detected the OD as the brightest region and outlined an imaginary circular approximation of the OD. Fischler and Bolles [50] found the boundary of OD by warping shape on the thresholded image and predicted to increase accuracy by constraining model Random Sample Consensus.

Although methods in this category achieve less accuracy as compared to the freeform based approaches but that can be increased by increasing the training set and including energy information of the contour and other statistical measures. The addition of previous knowledge regarding PPA and optic disc and removal of blood vessels in the OD region can increase the accuracy in images which are affected by the disease.

2.1.8 Optic Cup Extraction

For the detection of glaucoma, the most important features for the detection of glaucoma are CDR and NRR loss. Extraction of optic disc and the optic cup is required for the computation of these features. Extraction of the optic disc is also a difficult task because of the absence of any clear boundary and the presence of artifacts such as brightness and contrast variations. In some images boundary of the optic cup appears in the form of gradient and because of that manual detection of cup boundary even by specialist ophthalmologists shows lot of variations. To get the best segmentation evaluations of the algorithm, many researchers use the average boundary by different ophthalmologists. For the segmentation of cup many variations of ACM were applied

by researchers but because of lack of clear boundary, those efforts didn't produce quality results as some boundary points are required for the initialization of ACMs. Xu et al. [47] used the ACM model for the optic cup but to achieve that segmentation they use 3D fundus images instead of typical 2D images form digital fundus camera. As optic nerve is actually a 3D structure so they use depth parameter for the energy minimization according to shape and intensity. But this method is not much practical because for the evaluation of glaucoma 3D technology is not that common, furthermore, it increases the cost of capturing by many folds s compared to typical 2D images. In the literature, many researchers adopted a practical approach and presented their work on the 2D images for an extracting cup and CDR calculation.

2.1.9 Morphology-based approach

Nayak et al. [33] determined that green channel contains much information about the optic cup so for extraction of the cup they applied morphological operation on the green channel and used their algorithm for glaucoma detection by measuring CDR, NNR loss, and vascular shift. Babu and Shenbagadevi [39] proposed their methodology which involves removal of blood vessels from the image followed by the application of wavelet transformation on the green channel of the image. As the final step they used Fuzzy C-mean clustering on the resulted image. For the evaluation of their method they made a comparison of calculated CDR value with the ground truth values, obtained from the ophthalmologists. But they did not reported the segmentation accuracy of Optic disc and cup.

2.1.10 Level Set Approach

Wong et al. [54] represented the cup boundary in the form of the equitation of gradient flow by using level-set approach. They define the threshold from the normalized intensity values of green channel image and this threshold was used for the initialization of the equation of gradient flow. To reduce the roughness of the detected boundary they applied ellipse fitting to attain smoothness. For the extraction of the disc they followed the same method but use red channel instead of green. They extended their research on

cup extraction and proposed the use of kinks of blood vessels for cup segmentation which lies close to the edge of optic cup [55]. Their proposed methodology uses wavelet transformation and canny edge detector for the detection of cup edges. They experimentally determined 20° angle of vessel bending at the edge of the cup. 60 also used the information of vessels bending at the border of the optic cup and to achieve cup segmentation they use spline interpolation as the 3rd dimension and approximated the boundary of the optic cup by using knowledge about cup acquired from the 3D fundus images.

In the area of cup segmentation a very limited number of algorithms have been proposed in the literature and those already presented methods are just the starting point in this area. Some research is required for the determination of another parameter to distinguish the boundary of the optic cup. Furthermore, the introduction of a strategy to remove vessels in the OD region could improve the performance of the existing systems. Thus, the cup segmentation of cup is a wide research area that requires more efforts to achieve the state of the art methods to achieve reliable diagnosis systems for retinal diseases like glaucoma and DR.

Chapter 3

Materials

The proposed methodology is evaluated on five publicly available retinal image databases and one local database.

3.1 DRIVE

DRIVE [56] is a publically available database consisting of 40 images with resolution 584×565 pixels. Out of these 40 images, 7 are pathological, containing pigment epithelium changes, exudates, and hemorrhages.

3.2 DIARETDB1

The DIARETDB1 [57] database comprised 89 fundus images which are obtained with a 50° of FOV using a fundus camera and are in PNG format. These images are of size 1500×1152 pixels, with 24bits/pixel.

3.3 CHASEDB1

The CHASEDB1 [58] database consists of 28 images captured from a Nidek NM 200D camera at 30° FOV. Images are of 1280×960 pixels resolution, which is affected by illumination artifacts and poor contrast.

3.4 DRIONS-DB

The DRIONS [37] database consists of 110 images of 600×400 resolution, with 8 bits/pixel. In these 110 images, 50 images contain some sort of defects, such as

illumination artifacts, rim blurredness and papillary atrophy, which may hinder the detection and segmentation problem.

3.5   Messidor

The Messidor [59] database consists of 1200 retinal fundus images which were captured from 3CCD color video camera on Topcon TRC NW6 non-mydriatic retinograph, with 45° of FOV.

3.6   ONHSD

The ONHSD [16] database consists of 99 fundus images of 640×480 resolution. Images were captured from canon CR6 45MNf camera with 45° of FOV. Images were acquired from 50 patients, 19 out of which were diabetic.

3.7   Shifa Database

This database belongs to Department of Ophthalmology, Shifa International Hospital Islamabad, Pakistan. 19 images are healthy while the rest of them have some sort pathological symptoms and illumination artifacts. The dataset consists of 111 fundus images of 1936×1296 resolution, acquired with a 45° field of view.

3.8   Drishti-GS

Drishti-GD [60] consists of 101 fundus images of 2896×1944 resolution. All the images were disc centered, captured at 30° of FOV and saved in uncompressed PNG format. Images were taken from patients between the ages of 40 to 80 years. Four experts from ophthalmologic department established ground truths for these images. These ground truths involve segmented average cup and disc boundary, CDR value, and NRR notching site. These experts were well experienced, 3 to 20 years, in their field.

3.9   Ground Truths

The OD in all the images from the above-mentioned databases is hand labeled by ophthalmic experts from the Armed Forces Institute of Ophthalmology, Rawalpindi,

Pakistan and used as ground truths. These manual labeling of ground truths was performed by using boundary marking tool from our earlier research work [61]. For 1200 images in the Messidor database, we have used the ground truths provided by Aquino et.al [36]. The quantitative results are based on a comparison of automatically segmented images with these ground truths.

3.10 Quantitative Performance Measures

The outcome of OD detection and the segmentation process results in the classification of pixels belong to OD region or non-OD region. There are four possibilities for pixel classification, illustrated in Table 1, True Positive (TP), True Negative (TN), False Positive (FP) and false Negative (FN). The first two are the result of mutual agreement between predicted values and actual values while the last two are the result of the wrong prediction. TP is the case when the system predicts the pixel belongs to the OD and is actually an OD pixel in reference to the ground truth image while in the case of TN both the system and actual ground truth identifies a pixel as a non-OD pixel. FP is the case where the system predicts the pixel as an OD pixel when it actually belongs to the non-OD region in ground truth, whereas, in the FN case the system predicts a pixel as a non-OD pixel when it actually is an OD pixel.

The metrics used to evaluate the quantitative performance of the proposed methodology are given in Table 2. We used Sensitivity (SN), Specificity (SP), Accuracy (Acc), Positive Predicted Value (PPV), False Discovery Rate (FDR) and Overlap. The overlap metric is defined in (8).

$$\text{Overlap} = \frac{Area(ground\ truth \cap predicted)}{Area(ground\ truth \cup predicted)} \qquad (1)$$

Moreover, we have used the DICE similarity index to measure the similarity between the segmented optic disc and the ground truth. The DICE index is a measurement of spatial overlap used widely for comparing segmentation results, with a value ranging from 0 to 1. The DICE coefficient can be defined as two times the volume of the intersection between two segmentations divided by the sum of the volumes of the two segmentations, which is represented in (9).

$$DICE = \frac{2 * Area(ground\ truth \cap predicted)}{Area(ground\ truth) + Area(predicted)} \qquad (2)$$

Table 1 Pixel classification

Real → Predicted ↓	Actual pixel ∈ OD	Actual pixel ∉ OD
System Predicted pixel ∈ OD	TP	FP
System Predicted pixel ∉ OD	FN	TN

This work presents an OD detection and segmentation methodology which is able to detect the OD center without using any template or prior vascular information, an extension to our earlier work [62]. The OD appears as a yellowish structure in retinal fundus images with shape varying from circular to slightly elliptical and has the highest intensity value pixels. However, the presence of brightness artifacts can make the OD merge into the background and lose its brightness. Furthermore, the presence of several pathological structures such as exudates may take the shape of the OD and may have the highest intensity value. The proposed algorithm is based on morphological operations, Circular Hough transform and Grow Cut algorithm. The morphological operators are used to enhance the optic disc and remove the retinal vasculature and other pathologies. The optic disc center is approximated using the Circular Hough Transform, and the Grow Cut algorithm is employed to precisely segment the optic disc boundary.

Table 2 Performance metric for OD Segmentation

Measure	Description
SN	TP/(TP+FN)
SP	TN/(TN+FP)
Acc	(TP+TN)/(TP+FP+TN+FN)
PPV	TP/(TP+FP)
FDR	FP / (FP+TP)

Chapter 4

Methodology

4.1 Block Diagram

The project is divided into small modules in such a way that each module perform the subtasks of the project. This breakdown was done to make it extensible for the future work. Figure 4-1 shows different modules which are involved in the processing of diagnosis system.
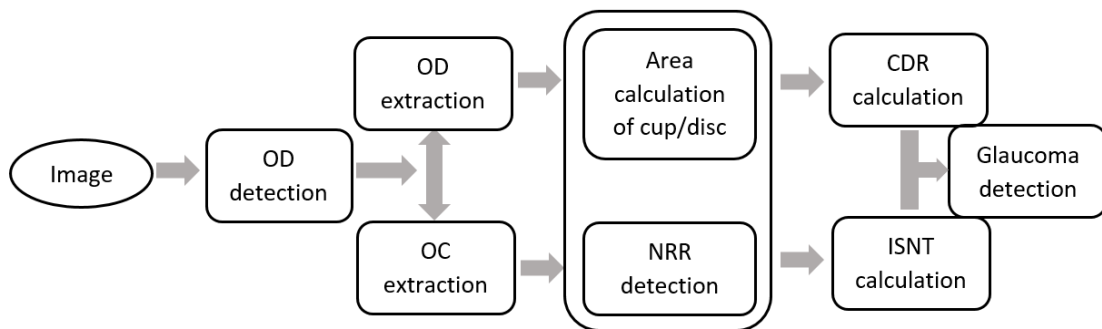
Figure 4-1 Proposed methodology.

4.1.1   OD Detection

This module deals with the detection of OD area from the image which was assumed to be circular in shape. The input of this module is the illumination corrected preprocessed fundus image and the first step of this module is the minimizing the vessel affect in the image. The second step involves OD detection by assuming it as a circular object. The output of this module is the detected OD center coordinates.

4.1.2   ROI Determination

The function of this module is to determine the region of interest (ROI) which is basically the brightest part of the image and it will be extracted on the basis of intensity value. The input to this module is the retinal fundus image of a person and its output the ROI of the image.

4.1.3   Optic Disc Extraction

This module involves segmentation of OD by using Grow Cut algorithm. The module takes the OD center coordinates as input and initialize the seed for GC algorithm. The pixels close to the detected center coordinates are assumed as foreground while pixels which are far apart are assumed as background. Algorithm assigns a label to each pixel and ultimately segment the whole disc. In the final step of this module, an approximation of the segmented boundary is performed by using an ellipse equation.

4.1.4   Optic Cup Extraction

This module takes the input from OD detection module and extract RIO from the image. The purpose of extracting ROI is to reduce the computational cost. The next step is the application of SLIC algorithm to create superpixels, which is followed by the feature extraction, training of ensemble classifier, and optic cup extraction. The output of this module is the segmented optic cup.

4.1.5   Disc and Cup area Calculation

This module calculates the area covered by OD and OC. The output of this module is calculated area.

4.1.6   NRR detection

This module takes the segmented OD and OC image to detect NRR. The output of this module is the detected NRR region.

4.1.7   CDR Calculation

This module takes the segmented optic disc and optic cup as an input and calculate cup to disc ratio, which involves vertical CDR, horizontal CDR, and CDR area.

4.1.8   ISNT Identification

This module uses the detected NRR to calculate ISNT notching site. The output of this module is the NRR notching site, inferior, superior, nasal, or temporal.
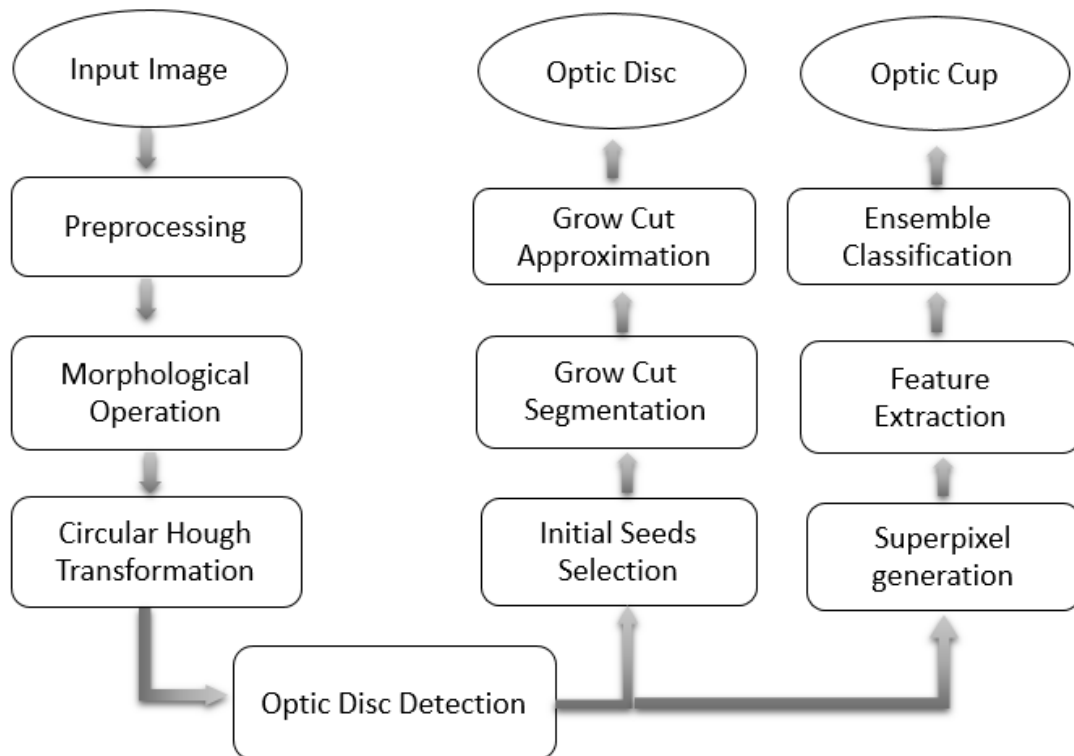
Figure 4-2 Steps for disc and cup segmentation.

4.1.9   Glaucoma Detection

This module makes decision about glaucoma presence. This module takes the input from CDR and ISNT module, compare the values with the normal specified range, and detect the extent of glaucoma progression in that image.

4.1.10   Implementation Details

For making decisions about the presence of glaucoma, extraction of optic disc and the optic cup is the first step towards detection process. The segmented disc and cup help in the calculation of CDR and ISNT, which are the two most important parameter to address glaucoma progression. ISNT rule makes the use of detected NRR to detect its notching site and make a decision on the basis of that. Figure 4-2 shows all the steps which are involved in processing.

4.1.11 OD Extraction

This module is used for the segmentation of the optic disc. This module undergoes several steps which are involved in carrying out the disc and cup segmentation process. OD detection is the primary step which is required to carry out segmentation.

4.1.12   Preprocessing

The variation in image contrast, background illumination and pigmentation is normalized by applying pre-processing operations to the retinal images.

The green channel of an RGB image gives maximum contrast between exudates and the neighboring regions [63]. Therefore, the green channel of RGB images is processed for normalization of contrast and luminosity. A variety of algorithms for contrast and luminosity normalization in retinal images are available in the literature, and these methodologies are either based on subtracting the estimated background from the original image [64] or on dividing the later by the former [65, 66]. However, our earlier work [64] shows that the results of both methods are similar with no appreciable advantage of one over the other. We have used the subtractive method as it has been reported in our earlier work [64]. The background pixel intensities are estimated and the difference between the estimated background and the green channel is computed to produce the normalized image. The background of the retinal image denoted as "Ibg" is estimated by applying a filtering operation with an arithmetic mean kernel. The size of the filter kernel is not a critical parameter as long as it is large enough to ensure the blurred image contains no visible structures such as an optic disc, exudates or blood

vessels. In this work, we have used an 89×89 pixel kernel. The difference between the estimated background "Ibg" and the morphologically opened image "Iopen" is calculated on a pixel basis. Thus, the background normalized image "Inorm" is obtained using:

$$I_{norm}(x, y) = I_{open}(x, y) - I_{bg}(x, y) \quad (3)$$

(a)   (b)   (c)

(d)   (e)   (f)
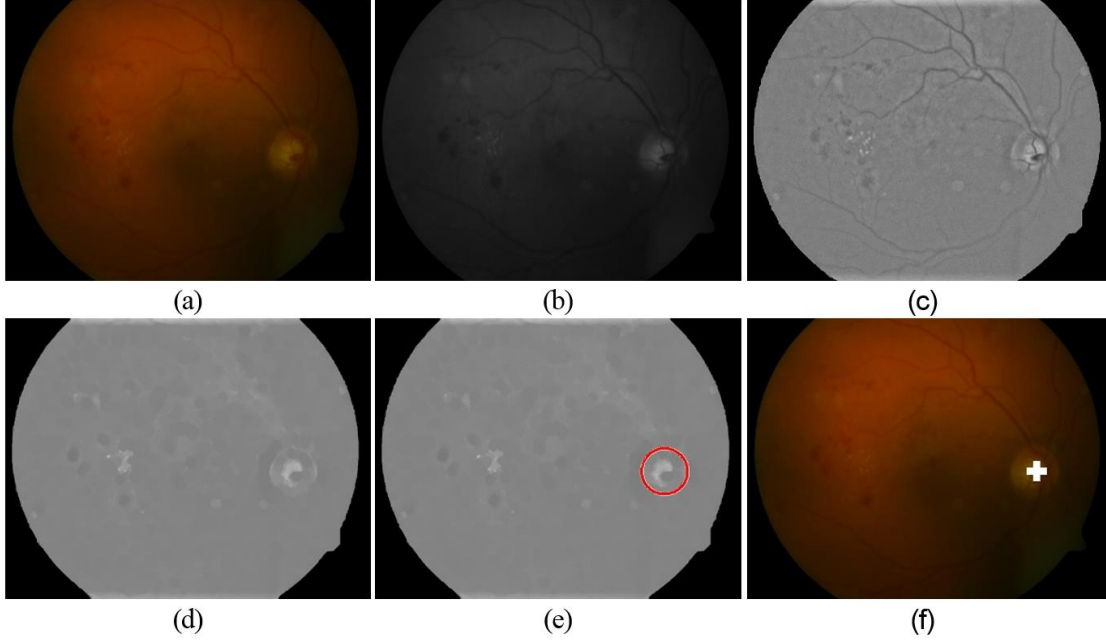
Figure 4-3 Processing steps for OD detection [67]

(a) RGB retinal image (b) Green Channel image (c) Preprocessed green channel image (d) Blood vessel removed image (e) Circular approximation of optic disc by CHT (f) Detected OD center

Due to different illumination conditions in the acquisition process, there may be significant intensity variations between images. These intensity variations make it difficult to use the best possible technique for all of the images, thus, shade corrections were necessary and have been applied. A global linear transformation function is applied to modify the pixel intensities.

$$I_{SC}(x, y) = \begin{cases} 0 & if\ I_{norm}(x, y) < 0 \\ 1 & if\ I_{norm}(x, y) > 1 \\ I_{adjusted}(x, y) & otherwise \end{cases} \quad (4)$$

$$I_{adjusted}(x, y) = I_{norm}(x, y) - IntVal_{MaxPixels} + 0.5 \quad (5)$$

Where $^{\text{Isc}}(x,y)$ is the shade corrected image, $\text{I}_{norm}(x,y)$ is the background normalized image, $^{\text{IntVal}}_{MostPixels}$ is the intensity value representing the most number of pixels in the normalized image $\text{I}_{norm}(x,y)$. Pixels with this intensity value $^{\text{IntVal}}_{MostPixels}$ represent the background [68]. This global transformation function normalizes or shade corrects the image by setting the background pixels to 0.5, which can be observed in Figure 4-3(c).

4.1.13 Optic Disc Detection

After pre-processing, the OD appears as the brightest structure in the image with varying size and appearance. The retinal blood vessels originate from the OD and branch out to spread in the retinal image. A morphological closing operation with a disc shaped structuring element is applied to the pre-processed image in order to remove the vasculature from the image. The result is shown in Figure 4-3(d).

CHT, an extension of Hough transform (HT) [69], is for the detection of circular objects from the image. For the detection of a circle, the HT is based on the equation of circle, defined as

$$(x_i - a)^2 + (y_i - b)^2 = r^2 \quad (6)$$

Where, "(a, b)" represents the coordinates of the center of the circle and "r" denotes the radius. In order to increase the performance of CHT, we resize all images to a common resolution and search for the bright circles with an experimented selected radius range of 29 to 50 pixels. To avoid false detection of OD we optimized our system by applying CHT on each image at different sensitivity levels and among circular responses generated by CHT we take only strong circle. Strong circles are the ones that correspond to the OD while the rest are either exudates or misleading regions. The results of intermediary processing steps for OD localization/detection are shown in Figure 4-3.

4.1.14 Optic Disc Segmentation

In the preprocessed image, the OD area is treated as foreground (fg) and the rest of the retinal image is considered as background (bg). The Grow Cut (GC) [70] algorithm separates the fg from bg using the von Neumann Neighborhood principle [71] and seeded region growing. The detected OD center is chosen as initial seed points for fg

area whereas the bg seed points are automatically chosen from rest of image. This algorithm iteratively checks each neighboring pixel and decides its region-wise membership.

The GC algorithm uses cellular automata for image modeling. Each image pixel "p" can be represented by a triplet (lp, θp, Cp). Where, "lp" represents the class label of the pixel "p" to which it belongs, "θp" represents the "strength" of the pixel "p" which is a measure of the certainty of the pixel "p" that should be labeled as "lp". The label of a pixel whose "strength" = 1 cannot be changed during the algorithm progress, whereas the pixel label whose "strength" < 1 may change during algorithm execution. "Cp" represents the pixel greyscale value.

At the initial stage of the algorithm, the triplet for all pixels is set as,

$$l_p = 0\ ,\theta_p = 0\ ,C_p =\ RGB_p \quad (7)$$

Which means that initially all pixels have undefined labels and zero strength. The aim of the GC algorithm in segmenting the OD is to assign a label to each pixel in the image regarding whether it belongs to OD or to the retinal image background. To start the algorithm, we initialized seeds by setting labels for the optic disc (+1) and non-OD (-1). Once the seeds are initialized, the process keeps on iteratively assigning labels to each pixel in the image until all pixels are labeled. For each pixel p and its neighbors xi (i=1 to 8), quantity "g" is computed which is monotonous decreasing function where g (xi) ∈ [0, 1] such that

$$g(x_i) =\ \frac{\|C_p - C_{xi}\|_2}{max\|C\|_2} \quad (8)$$

As we were using the green channel of the image so $\|C_p - C_{xi}\|$ is equal to $\|I_p - I_{x_i}\|$, where I_p and I_{x_i} are the intensities of pixels p and xi respectively. $max\|C\|_2$ is equal to 2L -1, where L is the bit depth of the image. Afterwards, the algorithm iteratively compute λ (xi) for all pixels xi which don't have label "undefined" such that:

$$\lambda(x_i) = g(x_i).\theta(x_i) \quad (9)$$

If $\lambda(x_i) > \theta_p$ then a pixel takes the label and strength of xi otherwise it keeps its own label and "strength". The algorithm terminates when all the pixels are labeled and the pixel label stops changing. In the end, the segmented OD boundary is approximated to an elliptical shape by using ellipse equation which involves drawing of ellipse outline over the segmented boundary of GC. The processing steps of OD boundary extraction are shown in Figure 4-4. The circular approximation of the OD boundary is illustrated in Figure 4-5.
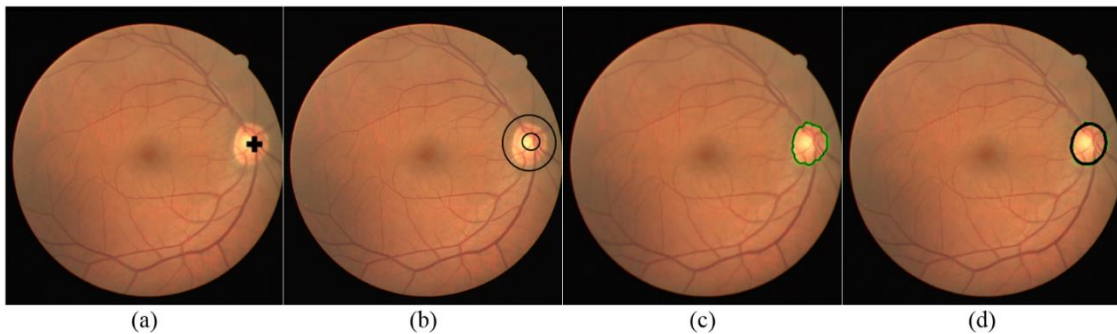

(a)   (b)   (c)   (d)

Figure 4-4 Steps for OD boundary extraction

(A) Original RGB image with detected central point of optic disc, (B) Foreground (optic disc area represented by small circle) selection points and background (non-optic disc region represented by large circle) selection points (C) Result of Grow Cut for boundary segmentation, (D) Boundary approximation (in black) of grow cut [67]

(a)   (b)
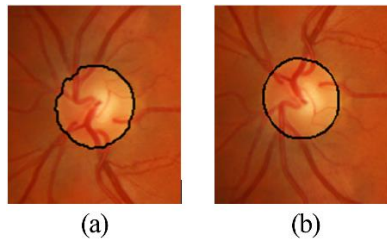
Figure 4-5 Close up view of (a) Grow Cut segmentation; (b) approximation of Grow Cut [67]

4.2 Optic Cup Segmentation

As optic disc don't have any clear boundary so information about the depth of optic cup helps the extraction process but this information is only available in the case of 3D fundus images. So in 2D fundus images, the helpful features are the contrast variations within OD region and the point of the disc where vessel appears in the form of kink. OD

do not have any well-defined shape and that is why its extraction quite challenging specially in the case where contrast variations are not obvious, whereas, vessel kinks detection is also a difficult task as the image may possess more than one kinks which can lead to false results. These challenges left us in a situation where limited landmarks are available for carrying out the extraction process. To address all the concerns and after reviewing the previous works published by the researchers, we have come to the conclusion that only image processing techniques are not sufficient to accurately segment the optic cup especially in the tricky situations.
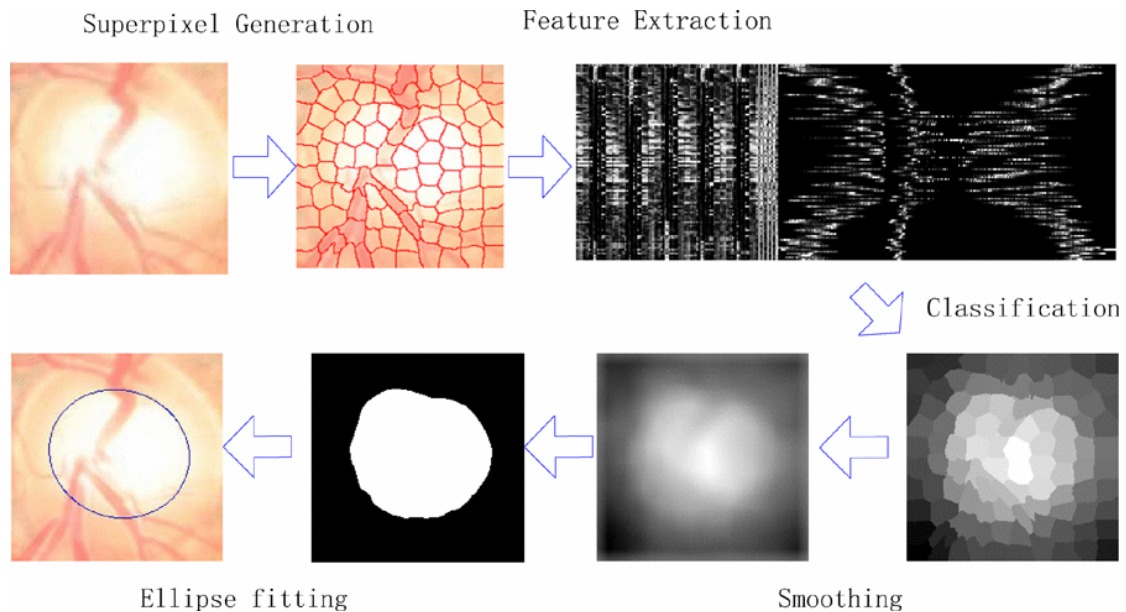
Figure 4-6 Steps for the extraction optic cup

In this work, we have applied supervised learning approach for the extraction of the optic cup and to achieve that we trained our classifier on the features extracted from superpixels of the training image sets. The idea of superpixels was incorporated for the first time in 2003 in the domain of machine learning and later with the advancement of time researchers from other domains also took the benefit of the algorithm. May algorithms, related to superpixel generation, have been proposed but for this specific task, however, we used a state of the art Simple Linear Iterative Clustering (SLIC) [32] algorithm which is one of the best in terms of processing, efficiency, and accuracy. After the application of this algorithm, the resultant image is divided into the set of superpixels

which give meaningful information about the structures present in the image and make it easy to analyze and extract specific features. After feature extraction, we trained our classifier and performed the segmentation of optic cup from the test images. Figure 4-6 shows the overall process of optic cup extraction. For multivariable classification ensemble classifier perform better classification as compared to other classifiers [58, 72]. We used bagging method of ensemble classifier for the classification of four classes, which are, optic cup, optic disc, blood vessels, and background.

4.2.1 Superpixel generation

Superpixel generation step was the most important step in cup segmentation process as the feature extraction step is based on the accurately generated superpixels. As mentioned earlier, we have used state of the art SLIC algorithm for that purpose because it has many advantages, over the other existing methods, like accurate boundary adherence and efficiency in terms of memory usage. Memory efficient algorithms always very help in medical image processing because those type of images are very complexed and have minor structures which help in the development of automated diagnosis systems.

SLIC algorithm takes a number of required superpixels N and smoothness as input parameter and on the basis of N it forms clusters k on a space grid where the center C_k of each cluster is separated by $S = \sqrt{(N/K)}$ pixels. It use 3×3 neighborhood to calculate gradient and move the center of each cluster in the direction of lowest gradient. For each initial cluster, SLIC modify its initial clusters by searching for its matching pixel, in 3×3 neighborhood, on the basis of color and appearance of new pixel. The process of assigning a newly found pixel to a cluster and calculating modified center for that cluster is iterative and keep processing until the maximum allowed distance, between new center and initial center, is achieved or when no new matching pixel remain to include. The final step of the algorithm ensure intra-cluster connectivity. This step also enforce connection between clusters which are not adjacent. Figure 4-7 shows

the neighborhood of the superpixel. In this work, we have generated 300 superpixels in the ROI of 256×256 pixels with the smoothness factor of 7.
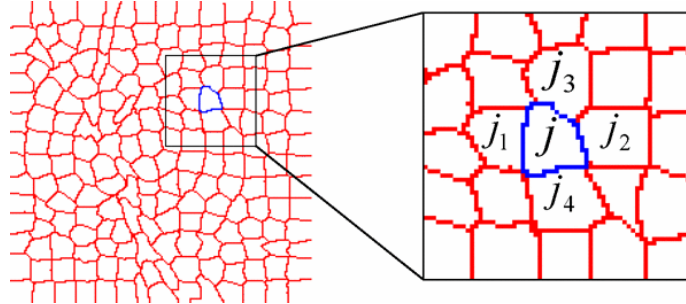

Figure 4-7 Superpixel neighborhood

4.2.2   Feature Extraction

The results of the supervised learning approach are dependent on the type of features and importance of the extracted from the image. Some features such as edges and lines are much simpler and are easy to extract but other features such as texture, color, appearance, and gist are much complex and required a great amount of work and processing. The accurately extracted features with great importance lead to the accurate segmentation of optic cup. For the purpose of cup segmentation extracted disc boundary is used to extract the cup features.

4.2.2.1   Contrast Enhanced Histogram

Optic disc boundary is not a case of a clear edge as it usually appears in the form of a gradient. So the main feature for extraction of the cup is the variation of color within the OD region and to extract that information we used a histogram of the g, b, s, and v planes of superpixel image. First, we divide the image into RGB color space and then into HSV plane but after examination, we determined that red color space is not the contributing factor in the cup segmentation process as it contains very little information about the cup which makes it consideration slim to none. Furthermore, the v plane from the HSV space is just like the red channel so we remove both r and v plane from histogram calculation step. As the medical images are usually affected by the contrast variations so to overcome that problem histogram equalization was performed

separately on green and blue channels but to avoid drastic effects of histogram equalization hue and saturation channels were not subjected to the process of equalization. Finally, the histogram calculations were performed separately for each channel. For the histogram calculation, 256 bins were used which made this vector of length $256 \times 4 = 1024$ which can be represented as

$$Hst_j = \left[h_j\big(HstE(g)\big)\, h_j\big(HstE(b)\big)\, h_j(h)\, h_j(s) \right]$$

Where HstE represents histogram equalization of specified channel and h_j represents the calculation of histogram from the jth superpixel. Figure 4-8 shows the six color channels which were initially considered for histogram calculation but as red and v channel have the same appearance and have no contribution for cup segmentation so they were removed from calculations.
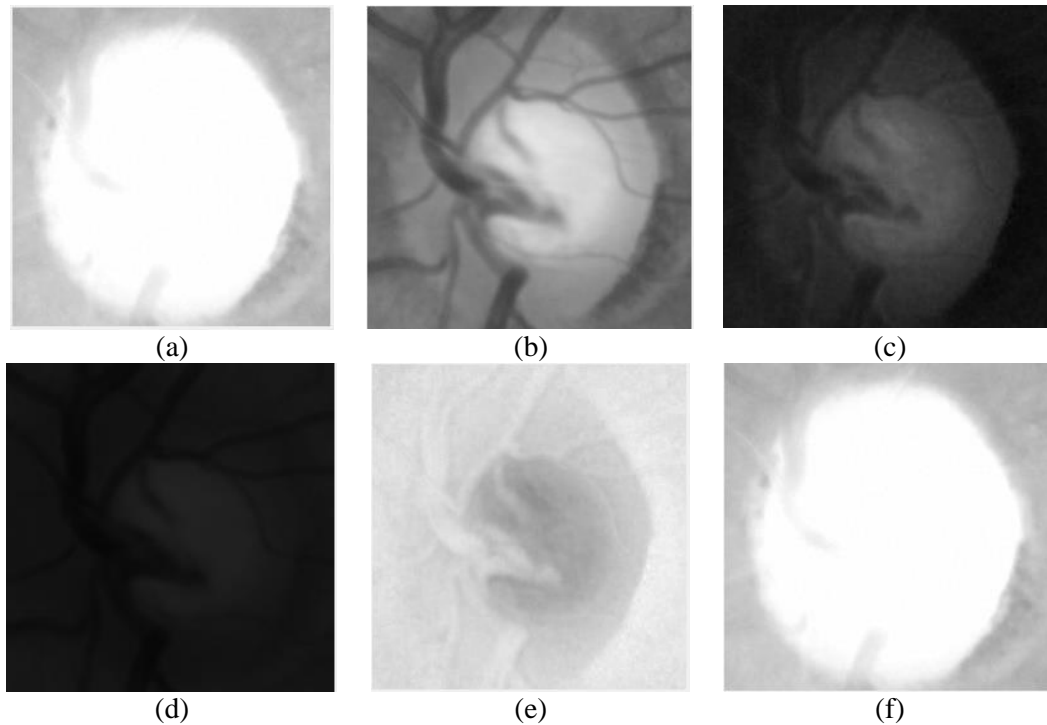

Figure 4-8 Image representation in RGB and HSV plane

(a) Red channel (b) Green channel (c) Blue channel (d) Hue space (e) Saturation space (f) Value space.

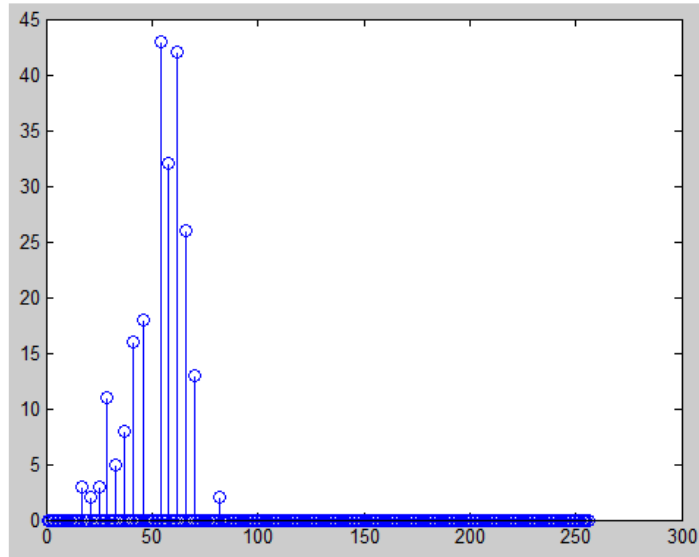Figure 4-9 shows the histogram of SP$_j$ which represents a histogram of one superpixel at location *j*.

Figure 4-9 One Superpixel histogram.

4.2.2.2   Center surround Stats (CSS)

For most of the cases, the boundary of optic cup is not clear as it appears in the form of gradient, which makes the segmentation highly complexed. In such situations first feature vector which was based on the histogram is not able to help the cup extraction so address that problem a CSS was introduced which was able to extract texture related information from the superpixels.

The computation of CSS is a two-step process, which is illustrated in Figure 4-10. The first step is the creation of 9 dyadic Gaussian pyramids, of the image, from level 0 (1:1) to level 8 (1:256). The result is just like low pass filtering where each coarser level has the lower frequency than its prior level. For the filtration process, a Gaussian filter is used with the division factor 2. This division helped the downsizing of the successive levels, as level 1 is downsized by factor 2 and level 8 is downsized by factor 2^8. The second step of this process involved the creation of 6 maps out of nine pyramids which were determined experimentally. To create them 3 finer levels C = {1, 2, 3} are selected as center levels while the coarser levels are selected by adding the distance of 3 and 4 in center level such that (S = c + d). Figure 4-10 shows all the 6 maps which are created between centers and surround levels. CSS is calculated for r, g, and b channel of

superpixel image. The feature map *m(c)* is used to represent center level map while *m(s)* represents surrounding level map. But before the calculation of CSS of these six maps interpolation of the surrounding level, represented as $|f_{c-s}(m(s))|$, is done to scale it up to the center level. Finally, the CSS is calculated for these maps, which is represented as $|m(c) - f_{c-s}(m(s))|$, and resizing of all maps to their original image size is done. Six maps for three channels (r, g, and b) made a total of 18 maps. $M_i = \{1\text{-}18\}$ represents the *i*th map and for each map mean (μ_j) and variance (var_j) is calculated for each superpixel (SP_j) as shown in the equation (9, 10).

$$\mu_i(i) = \frac{1}{n_j} \Sigma_{(x,y)\in SP_j} M_i(x,y) \qquad (9)$$

$$var_i(i) = \frac{1}{n_j} \Sigma_{(x,y)\in SP_j}(M_i(x,y) - \mu_j(i))^2 \qquad (10)$$
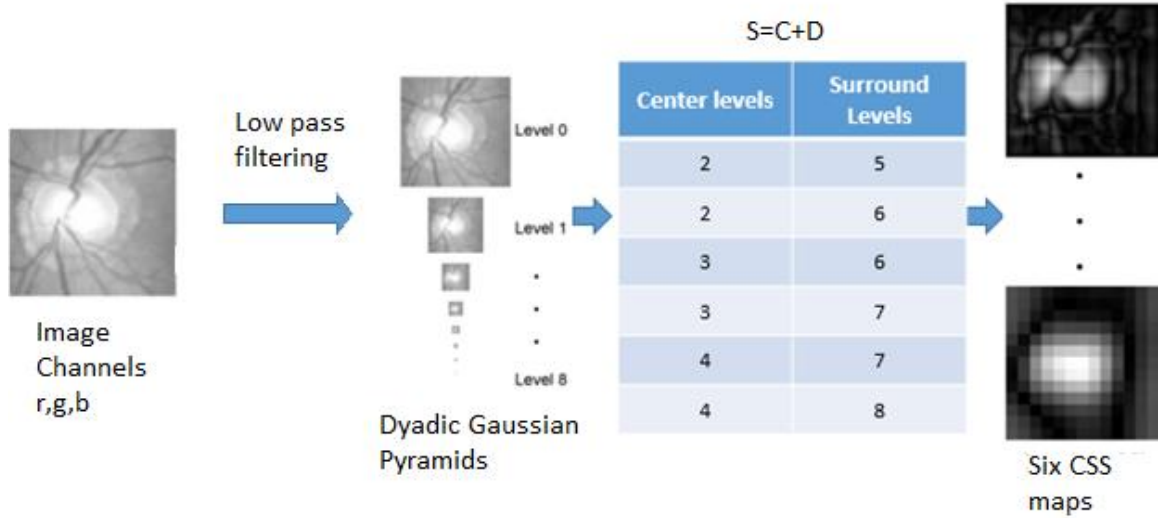
Figure 4-10 CSS calculation

4.2.2.3   Distance Feature

Distance D feature is used for the case of images where cup boundary is not obvious as this feature is based on the fact that cup is present at the center of the OD. For that purpose, a distance is added between the superpixel center and the OD center which is used to locate the cup, the process is shown in Figure 4-11. This normalized distance dynamically changes with the minor and major axis of the OD. The mathematical equation for the computation of OD is given below:

$$D_j = \sqrt{\left(\frac{x_c - x_j}{h}\right)^2 + \left(\frac{y_c - y_j}{w}\right)^2} \qquad (11)$$

Horizontal and vertical coordinates of disc center are represented as X_c and Y_c while X_j and Y_j are the center points of superpixel j, h and w denote major and minor axis of OD.

The final feature vector of optic cup is the combination of histogram, CSS, and distance vector which is represented as: [$HIST_j$ CSS_j D_j]
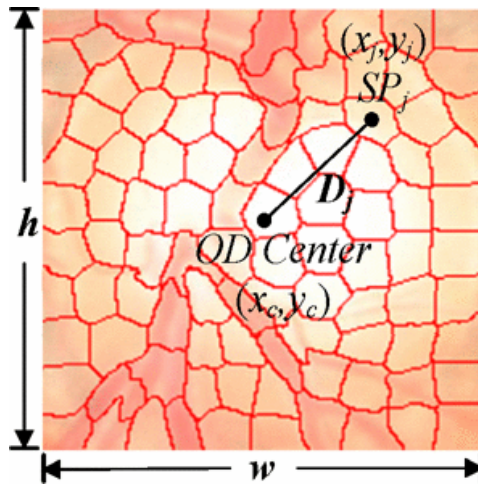
Figure 4-11 Introduction of distance between disc center and cup center.

4.2.2.4   Feature Reduction

The graph of predicted feature importance is shown in the figure. The cup final feature vector is of length 1205 but the analysis of graph expressed that some features have not contributed in the feature extraction for the purpose of cup prediction. The next step is performed for the reduction of vector length by removing unimportant features from the final vector which made the final reduced feature vector of length 695. Figure 4-12 and Figure 4-13 shows the importance of same feature vector on different ensemble methods. The bagging method of ensemble presents more importance to the feature used.
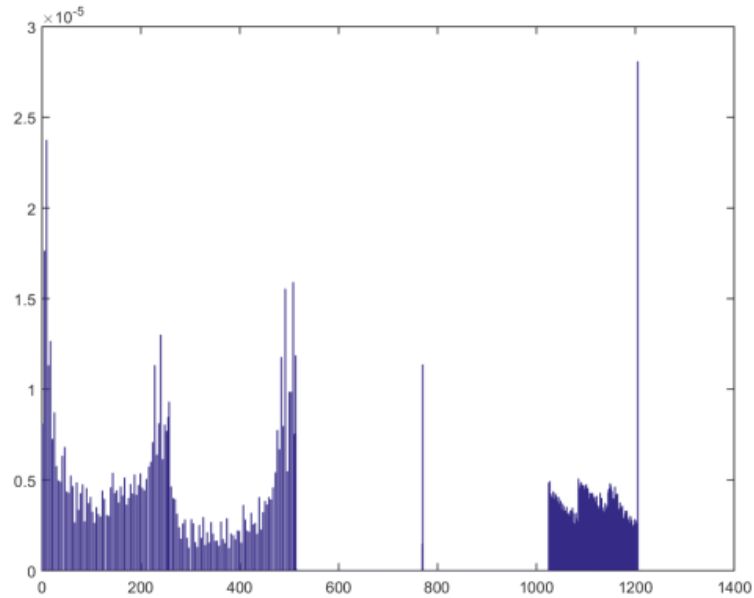
Figure 4-12 Feature vector of bagging

(a)   (b)
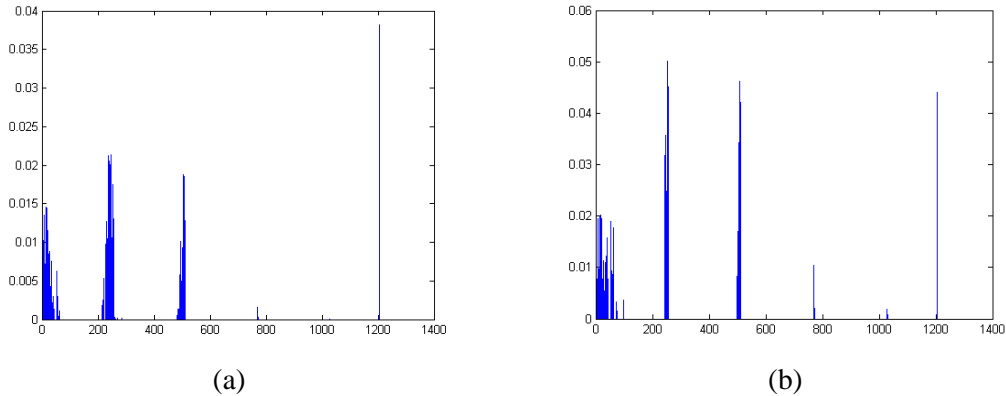
Figure 4-13 Feature vector for (a) AdaBoostM2 and (b) RUSBoost

4.2.3 Establishment of Training Set

For the training and cup boundary detection from the images, ensemble classifier is used with the bag method. The bagging method was empirically selected after using other ensemble methods like RUSBoost, AdaBoostM2, and subspace as bagging produce better detection of cup boundary based on the multiclass training set. Four selected multiclass features are a cup, nerves, disc, and nerves. For the establishment of the multiclass training set, a GUI based application is used which assign labels to these

structures as 1 for background, 2 for the disc, 3 for the cup, and 4 for vessels. The front end view of the GUI for ground truth is shown in Figure 4-14 where superpixels of the images are calculated and manual user click is used to assign different color labels to the cluster of superpixels. 35 images are used for the training of ensemble classifier under different iterations. All of these four classes are used for the training of the classifier and testing of the test images is performed on the basis of trained classification model.
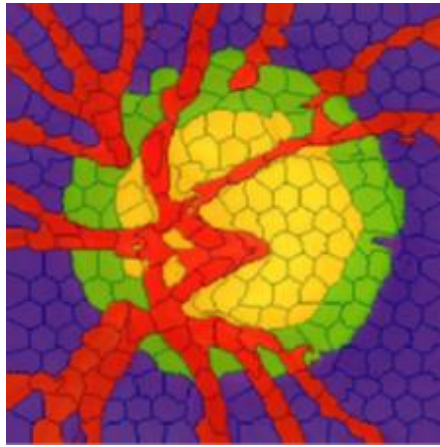
Figure 4-14 Feature extraction for establishing ground truths.

4.2.4 Classification of Superpixel for Estimation of Cup

In the process of testing of ensemble model on the test images, it gives the output of final decision value about each pixel. The pixels which belong to optic cup attain the decision value of two and intensity value of 255. The rest of the pixels belongs to the background and get the 0 intensity value in the binary image. The cup boundary in the binary image is then subjected to morphological opening and closing operation which allow maximum connectivity to the largest components and remove small components as shown in Figure 4-15. The connected components are used for the boundary estimation and finally the ellipse is detected by the use of ellipse Hough transformation. Five ellipses fitted boundaries are used to estimate cup boundary and the ellipse which fits best to the major axis of the segmented image is considered as the best fit as shown in Figure 4-16.

Figure 4-15 Cup boundary estimation by using image processing techniques

(a)   (b)
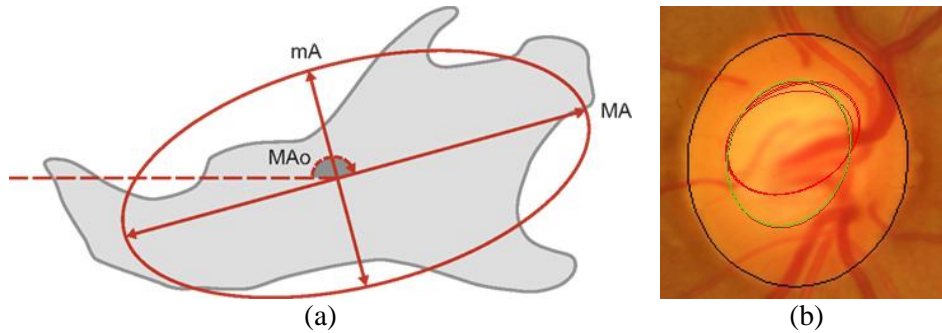
Figure 4-16 Ellipse fitting on segmented cup

(a) Usage of major and minor axis for ellipse fitting (b) raw (red) and fine (green) ellipse fitting on optic cup.

4.3 CUP to DISC Ratio

After the segmentation of disc and cup is completed, the segmented binary images are subjected to the CDR calculation module which determines the vertical CDR by using decimating the cup diameter to the disc diameter as $CDR=VCD/VDD$

The calculated CDR is used for making a decision about the presence of glaucoma. When the ratio exceeds the defined threshold value then it indicates the glaucoma progression.
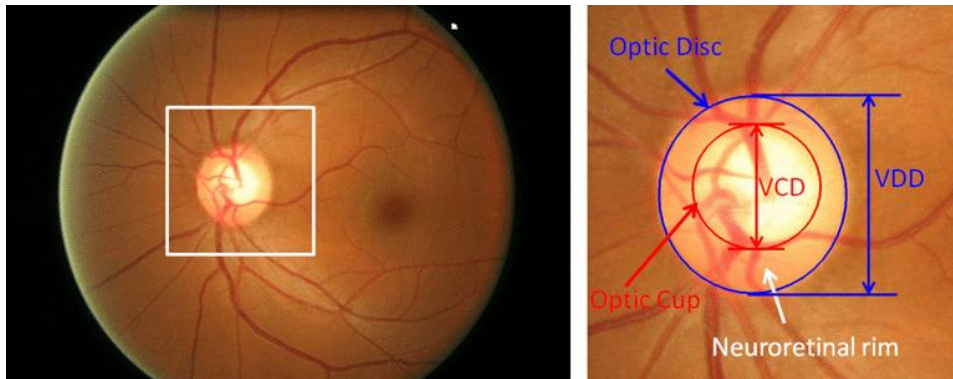
Figure 4-17 CDR Calculation from selected ROI.

Chapter 5

Experimental Results

5.1 Optic Disc Detection

The optic disc detection method achieved 100% success rate in DRIVE, DIARETDB1, CHASE_DB1 and Shifa databases, it achieved 99.09% in DRIONS-DB and 99.25% in the Messidor database. Table 3 shows the accuracy of this method for the detection of OD. The comparison of accuracy in localizing OD has been made with other methods reported in the literature in Table 4**Table 4**.

Table 3: Performance Measure of OD detection [67]

Datasets	Images	OD detected	OD missed	Accuracy
DRIVE	40	40	0	100%
DIARETDB1	89	89	0	100%
CHASE_DB1	28	28	0	100%
DRIONS-DB	110	109	1	99.09%
Messidor	1200	1191	9	99.25%
Shifa	111	111	0	100%
ONHSD	90	90	0	100%

Figure 5-1**Figure 5-1** shows the results of the OD detection in the DRIVE, DIARETDB1, Shifa, CHASE_DB1 and DRIONS-DB databases. The OD detection method can correctly detect the OD center even in the presence of exudates and other pathologies. Accurate detection of the optic nerve head facilitates the segmentation algorithm to extract the boundary with high precision.
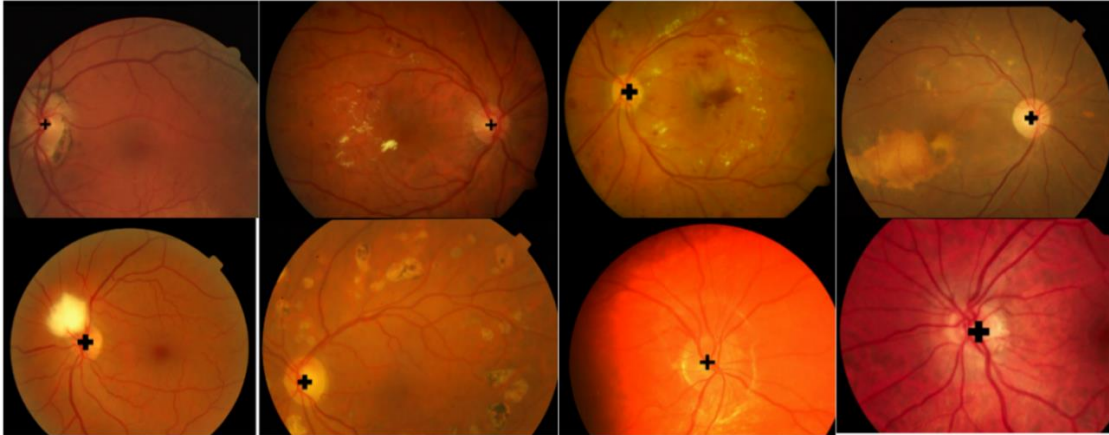
Figure 5-1 OD detection results. Sorting of images in rows is according to the following order DRIVE, DIARETDB1, Messidore, Shifa, CHASE_DB1 and DRIONS-DB [67]

Table 4: Comparison of OD localization with other methods [67]

Authors	Database	Accuracy
Youssif et. al. [24]	DRIVE	98.8%
Niemeijer et. al. [73]	Local database	99.4%
Aquino et al. [36]	Messidor	99%
Welfer et al. [74]	DRIVE	100%
	DIARETDB1	97.75%
Lu [75]	Messidor	98.77%
Zubair et al. [76]	Messidor	98.65%
Mahfouz & Fahmy [30]	DRIVE	100%
	DIARETDB1	97.8%
Yu et al. [77]	Messidor	99%
Saleh et al.[78]	DRIVE	100%
Yu et al. [79]	DRIVE	100%
	DIARETDB1	99.88%
	Messidor	99.67%
Proposed method	DRIVE	100%
	DIARETDB1	100%
	CHASEDB1	100%
	DRIONS-DB	99.09%
	Messidor	99.25%
	ONHSD	100%

5.2 Optic Disc Segmentation

The pixel-wise quantitative performance metrics (which are defined in Table 2) are calculated for OD segmentation, based on the comparison of automatically segmented images with the ground truth reference images and are illustrated in Table 5. The methodology is quantitatively evaluated by using an array of performance metrics, which to the limit of our knowledge has not been previously used for evaluating OD segmentation algorithms.

Table 5 Performance measures of OD segmentation [67]

Performance Measure	DRIVE	DIARET DB1	CHASE-DB1	Shifa	DRION S-DB	Messidor	ONHSD
Acc	0.9672	0.9772	0.9579	0.9793	0.9549	0.9989	0.9967
SP	0.9966	0.9984	0.9971	0.9991	0.9966	0.9995	0.9992
SN	0.8187	0.8510	0.8313	0.8015	0.8508	0.8954	0.8857
PPV	0.8728	0.9263	0.9261	0.9493	0.9966	0.9794	0.9619
FDR	0.1271	0.0737	0.0738	0.0506	0.0810	0.020	0.038
DICE	0.8720	0.8910	0.9050	0.8763	0.9102	0.9339	0.9197
Overlap	78.6%	85.1%	83.2%	80.1%	85.1%	87.93%	86.1%
Hausdorff	0.2514	0.1915	0.3174	0.2434	0.2578	0.1627	0.2245

The comparison of the proposed method has been made with other available methods on the basis of average sensitivity, specificity, accuracy, DICE score, overlap, positive predictive value and the time taken to process a single image, as illustrated in Table 6. Results show that the proposed method provides promising results as compared to other OD segmentation techniques in the literature. The comparison with other methods is made with respect to DRIVE and DIARETDB1, DROINS-DB, Messidor and ONHSD retinal image datasets.

Table 6 Comparison of OD segmentation with other methods [67]

Performance Measures → Methods↓	Sensitivity	Specificity	Accuracy	DICE Score	Overlap %	Predictive Value	Average Time per image (in sec)
DRIVE Database							
Sopharak et al. [80]	0.2104	0.9993	--	--	16.88	0.9334	14.92
Walter et al. [81]	0.4988	0.9981	--	--	29.32	0.8653	219.6
Seo et al. [82]	0.5029	0.9983	--	--	31.09	0.843	7.23
Kande et al. [83]	0.6999	0.9888	--	--	29.66	0.5218	111.7
Stapor et al. [84]	0.7368	0.9920	--	--	33.42	0.6198	43.00
Lupascu et al. [85]	0.7768	0.9968	--	--	30.95	0.88.14	--
Welfer et al. [86]	0.7357	0.9982	--	--	39.40	0.8876	53.65
Basit & Fraz [87]	0.8921	0.9921	--	--	61.88	0.6930	--
Morales et al. [88]	--	--	0.9903	0.8169	--	0.8544	--
Salazar-Gonzalez et al. [89]	0.7512	0.9684	0.9412	--	--	--	--
Proposed Method	0.8188	0.9966	0.9672	0.8720	78.6	0.8728	59.2
DIARETDB1 Database							
Sopharak et al. [80]	0.4603	0.9994	--	--	29.41	0.9593	74.55
Walter et al. [81]	0.6569	0.9993	--	--	36.97	0.9395	308.5
Seo et al. [82]	0.6103	0.9987	--	--	35.32	0.8878	15.63
Kande et al. [83]	0.8808	0.9878	--	--	33.41	0.5448	120.5
Stapor et al. [84]	0.8498	0.9964	--	--	34.08	0.8034	59.72
Lupascu et al. [85]	0.6848	0.9969	--	--	30.95	0.8117	--
Welfer et al. [86]	0.6341	0.9981	--	--	39.15	0.8704	57.16
Basit & Fraz [87]	0.7347	0.9944	--	--	54.69	0.7049	--
Morales et al. [88]	--	--	0.9957	0.893	--	0.9224	--
Proposed Method	0.851	0.9984	0.9772	0.891	85.1	0.9263	40.0
DRIONS-DB							
Walter et al. [81]	--	--	--	0.6813	--	--	--
Morales et al. [88]	--	--	0.9934	0.9084	--	0.9281	--
Proposed Method	0.8508	0.9966	0.9989	0.9102	85.1	0.9794	43.2
Messidor							
Morales et al. [88]	--	--	0.9949	0.8950	--	0.9300	--
Kumar et al. [90]	--	--	--	0.8456	--	--	--
Proposed Method	0.8954	0.9995	0.9989	0.9339	87.93	0.9794	71.3
ONHSD							
Morales et al. [88]	--	--	0.9941	0.8867	--	0.9310	--
Proposed Method	0.8857	0.9992	0.9967	0.9197		0.9619	65.3

Figure 5-2, Figure 5-3, and Figure 5-4 presents the graphical presentation of the comparison between two public databases, DRIVE, and DIARETDB1. The comparison has been presented on the basis of reported specificity, sensitivity, and overlap in Table

6. Graphical presentation of the data shows the trend of improvement of presented methods over the period of time.
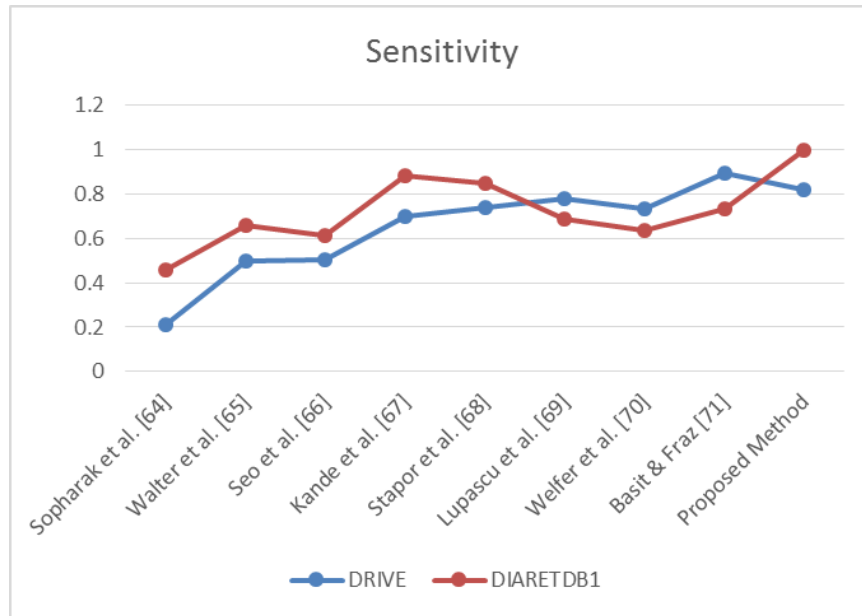

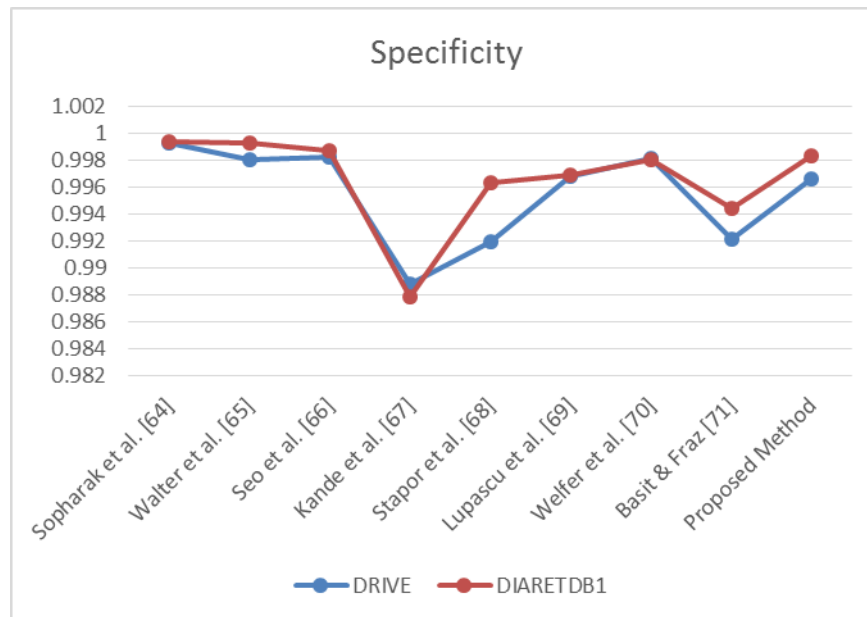Figure 5-2 Graph comparing sensitivity of proposed method on DRIVE and DIARTEDB1

Figure 5-3 Graph comparing specificity of proposed method on DRIVE and DIARTEDB1
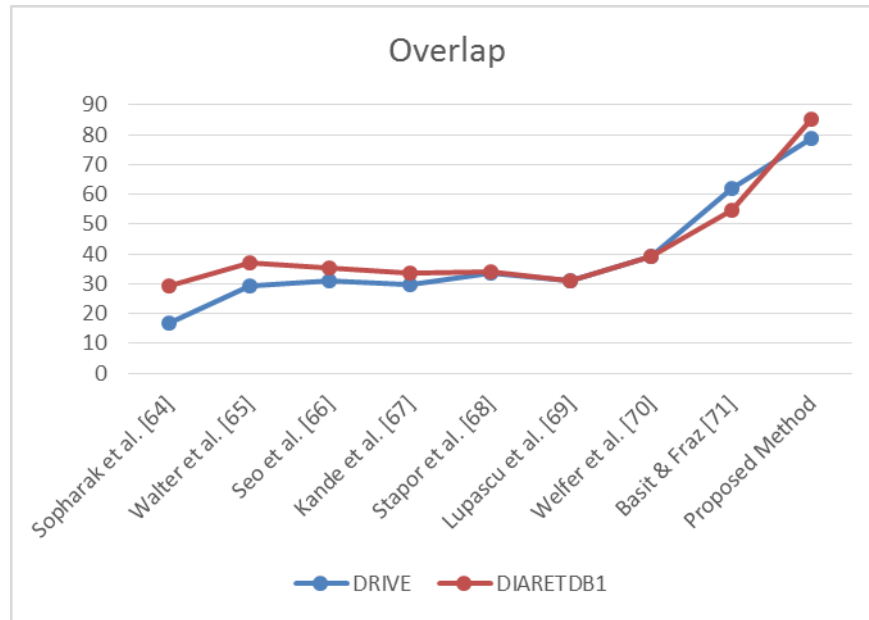
Figure 5-4 Graph comparing overlap percentage of proposed method on DRIVE and
DIARTEDB1

The OD segmentation results on these retinal datasets are illustrated in Figure 5-5. It
can be observed that the proposed methodology can successfully detect and segment the
OD in the pathological images as well as in images with non-uniform illumination and
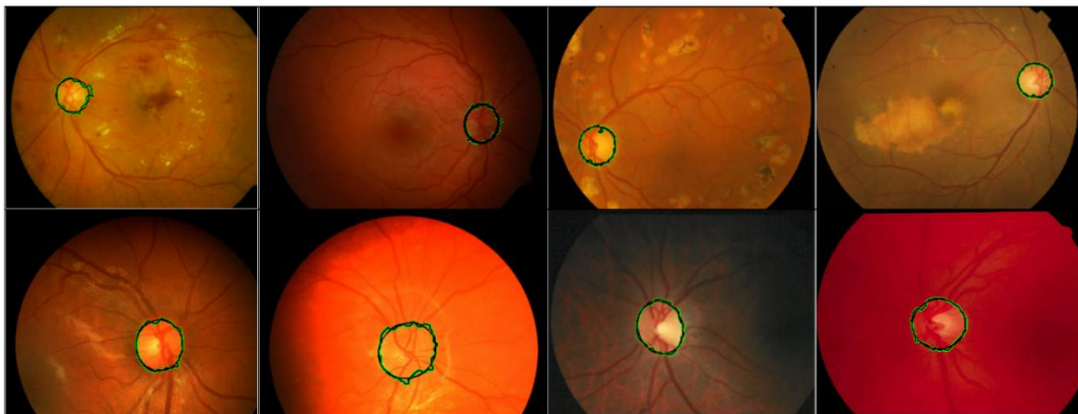uneven background pigmentation from multiple retinal image datasets.

Figure 5-5 Examples of segmentation. Images in each row belong to separate databases as per
order, DIARETDB1, Shifa, CHASE_DB1, and DRIONS-DB. Grow Cut segmentation is
represented by a green boundary and its final approximation is represented by a black circle
[67]

5.3 Robustness of Methodology

The robustness of proposed methodology has been evaluated on the basis of its OD localization and segmentation performance on (1) the noisy images, (2) the images with illumination artifacts, and (3) the images with pathological structures. The retinal images are corrupted with three types of noise models typically found in biomedical images (Gaussian, Salt & Pepper, and speckle noise). It can be observed in Figure 5-6, that OD is successfully detected and segmented despite the significant deterioration of the retinal images due to the addition of noise.
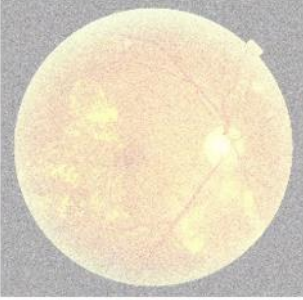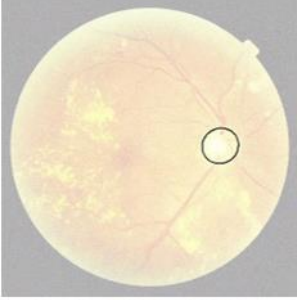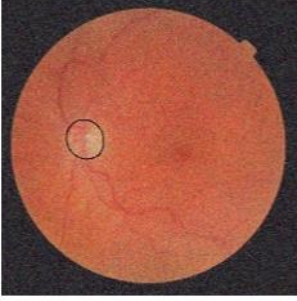

Figure 5-6 Performance in the noisy images [67]

Second criteria for measuring robustness is the evaluation of against illumination which makes OD detection harder because poor illumination hides the OD in the background, as a result of which segmentation algorithms fails to extract boundary. Figure 5-7 shows some extreme cases of poor illumination where proposed method successfully localize and segment the OD.

Pathologies such as papillary atrophy, exudates, and lesions put a potent threat to accurate segmentation of optic disc because some pathologies may appear in bright or in a circular shape and may result in misclassification. While others like papillary atrophy surround the OD and make it difficult to segment. Figure 5-8 shows the result of proposed algorithm on pathologically affected images.
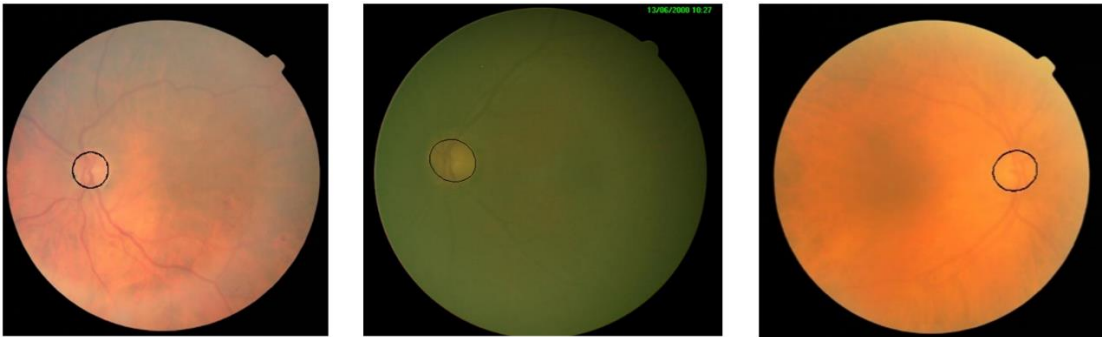
Figure 5-7 Performance in the poor contrast and uneven illumination [67]

Figure 5-8 Performance in the presence of pathologies [67]

Although algorithm works fine on images where segmentation is hard but in fundus imaging, sometimes, there are images which are poorly focused or have imaging artifacts which make segmentation a difficult task. Figure 5-9 shows some extreme

cases where method failed to extract optic disc correctly e.g. in the first two images the artifacts are so strong that it almost hide out OD and leaves false detection and segmentation while in the third image pathologies hide the boundary of OD and leave the method to partially detect OD.
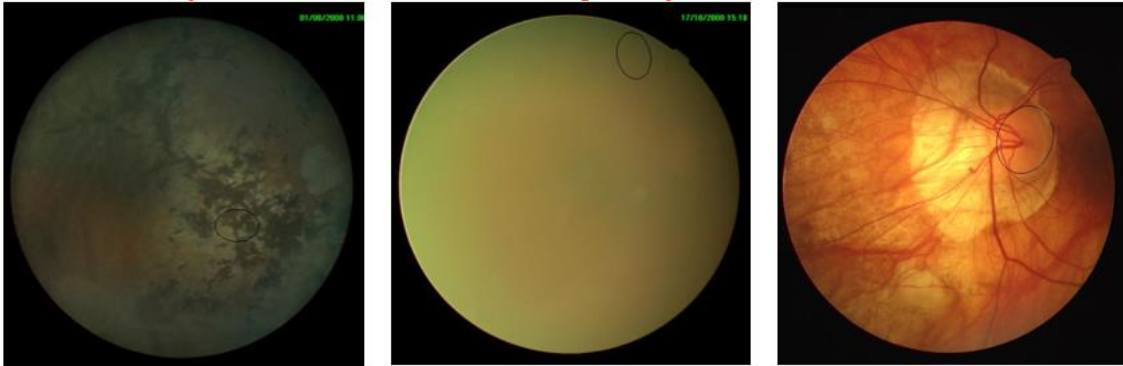
Figure 5-9 Incorrect OD segmentation in difficult cases of retinal images [67]

5.4 Optic Cup segmentation

The Drishti-GS1 database is used for the evaluation of this segmentation method. The evaluation of the method has been done at different learning cycles of the ensemble classifier which presented much better accuracy of about 97% as shown in Table 7. Figure 5-10 shows the results of cup segmentation.

The results of the CDR of the method is compared against the CDR provided by the four experienced ophthalmologists. The comparison of the CDRs is provided in Table 8. As already mentioned that boundary of optic cup is not prominent and in most of the cases it is based on the best guess of the experts and that is the reason that boundary detected by different experts shows significant variations. Figure 5-11 shows the performance of ensemble model at different learning. In ensemble, different bootstrap replicas of the dataset are produced and these replicas are used to breed the decision tree. The performance of the model is stable at different cycles but shows slight improvement between the ranges of 100 to 150.
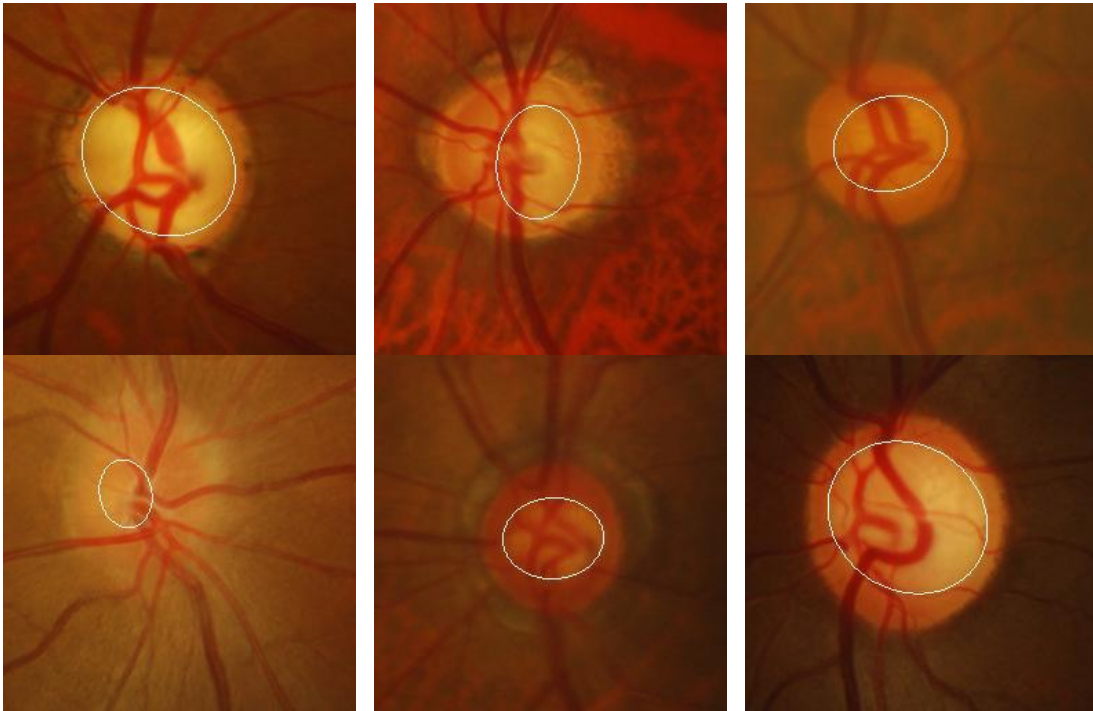
Figure 5-10 results of cup segmentation on the Drishti-GS1 database.

Figure 5-12 shows the probability of getting misclassified classification tree, which is denoted as the mean square error (MSE). To get MSE, ensemble model ranges from 20 - 200 decision trees is created on the basis of training dataset and MSE is calculated on these decision trees. The out of bag error shows decreasing trend with an increase in the number of decision trees. 5 fold cross validation of bagging based ensemble was created for the analysis of cross-validation error. The purpose of using this validation is to make a comparison of the independent dataset on the basis of their estimated value. The difference between out of bag classification error is very small, once it passes 80 weak learners, and it appears as an almost straight line. On the basis of this observation, the classifier is created on 150 decision trees in order to keep the balance between accuracy and computation time, as the computation time increases with the increase in the number of decision trees.

The values of CDRs is subject to change when it is observed manually by different experts. Table 8 shows the variations between the estimated CDRs by four different experts. Although none of them is wrong but the averaging the CDRs from four experts provide a good way to compare results.

Table 7 Performance measures of cup segmentation.

No. of learning Cycles	Accuracy	Specificity	Sensitivity	PPV	FDR	DICE	Overlap
20	0.966049	0.991218	0.689911	0.768082	0.231918	0.716659	0.677859
40	0.966885	0.991003	0.710939	0.777678	0.222322	0.739551	0.687047
60	0.965904	0.993028	0.694082	0.812528	0.187472	0.720922	0.679767
80	0.967814	0.992797	0.709925	0.793364	0.206636	0.740295	0.688532
100	0.967872	0.992416	0.725225	0.801039	0.198961	0.750559	0.690206
120	0.965650	0.991562	0.697798	0.760461	0.239539	0.716073	0.67173
140	0.971631	0.99701	0.721943	0.81926	0.18932	0.76942	0.72968
160	0.965929	0.99491	0.69563	0.79305	0.20351	0.75631	0.71636
180	0.966195	0.99573	0.70909	0.79396	0.20613	0.75743	0.69436
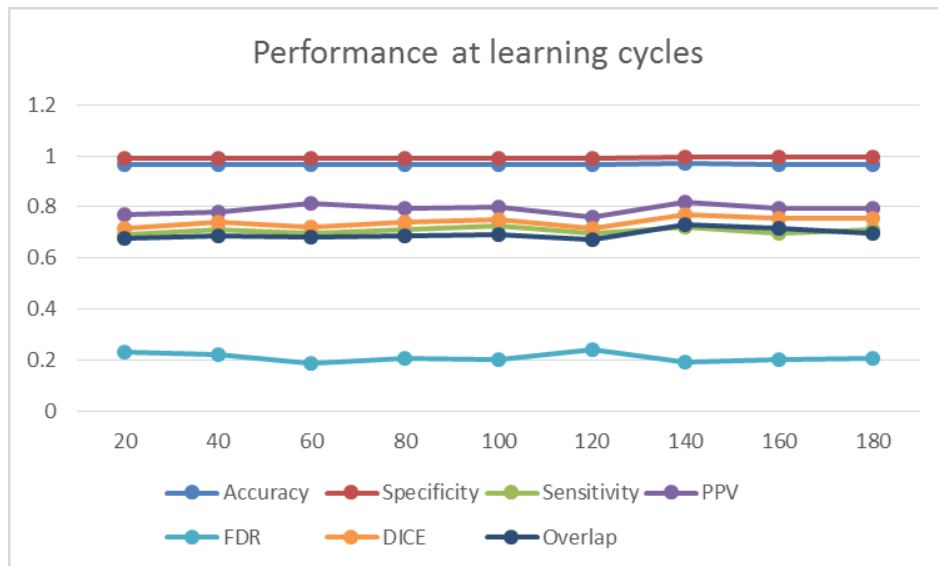
Figure 5-11 Performance evaluation at different learning cycles of ensemble
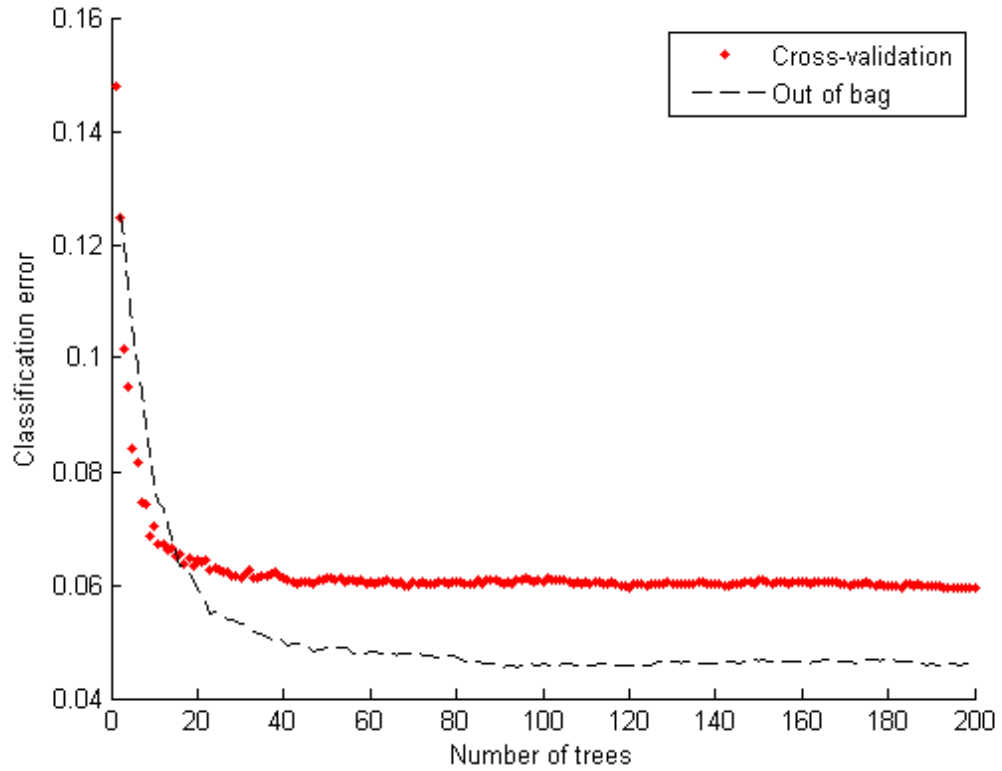
Figure 5-12 Out of bag error plot of test images for 200 ensemble models

Table 8 Comparison of CDRs with manually determined CDR by four experts.

Images	CDRs				
	Proposed method	Expert 1	Expert 2	Expert 3	Expert 4
drishtiGS_010	0.8702	0.95	0.85	0.88	0.88
drishtiGS_017	0.4615	0.36	0.60	0.63	0.54
drishtiGS_036	0.7500	0.70	0.76	0.71	0.72
drishtiGS_041	0.6000	0.55	0.71	0.63	0.53
drishtiGS_063	0.7801	0.78	0.77	0.78	0.76
drishtiGS_089	0.4508	0.38	0.52	0.47	0.42
drishtiGS_101	0.3519	0.37	0.37	0.33	0.31

Chapter 6

Discussion and Conclusion

Medical images are highly complexed and take a lot of time when the manual analysis is performed. Diagnosis of many diseases is performed on the basis of captured image e.g. magnetic resonance imaging (MRI), computed tomography scan, optical coherence tomography, and fundus imaging. With the advancement of technology and the introduction of best resolution cameras motivated the researchers to facilitate the doctors by providing automatic detection of diseases with the help of image processing and computer vision approaches. CAD systems gained the importance by the introduction of many states of the art methods which can automatically detect disease with much higher accuracy. Many of such proposed systems have been developed and serving the automated detection with small computation time. The simplicity of such systems made the operators of the cameras to diagnosis many diseases with much better precision.

As described earlier, fundus images present much better visual information about different retinal structures, furthermore, images capturing process is cheap and noninvasive. These properties of fundus imaging made it an excellent candidate for the development of CAD systems. Many diseases such as glaucoma, diabetic retinopathy, macular edema, retinal pigments, and some other diseases. Out of these mentioned diseases, glaucoma is the most chronic diseases which is the second leading cause of blindness after cataract. The problem with glaucoma is that it do not show symptoms at its early stage and detection at that point is possible through the retinal fundus imaging. That is why ophthalmologists advised each individual to screen once after few years to avoid complications which are associated with the prolonged disease condition.

The screening of large population is required to reduce the blindness cases in the community. For that purpose, manual diagnosis is not a good option as it takes much time and the presence of experts is required. To overcome this problem, researchers presented computer based

automatic diagnosis systems. But to achieve a state of the art methodology this is one of the main focus areas.For the detection of glaucoma segmentation of optic cup and disc is required to calculate CDR but the presence of pathologies is associated with the glaucoma presence and these pathologies hide the boundary of the disc, especially the PPA region. To overcome that problem we used a combination of image processing techniques to minimize the effects of pathologies and to achieve accurate optic disc segmentation. The second major task is the segmentation of optic cup which usually do not have any clear boundary and that makes image processing techniques difficult to extract exact boundary. For cup segmentation, we made use of supervised machine learning approach and for that purpose bagging method of the ensemble was empirically selected for training on the basis of extracted features from superpixels. Superpixels cluster the pixels which have some sort of similarity and for generation superpixel SLIC algorithm is used as it has better accuracy and boundary adherence. The extracted boundary from the cup is first subjected to morphological operations and then approximated by the elliptical Hough transformation.

Finally, the extracted boundary of optic disc from grow cut algorithm and cup boundary from ensemble classifier is used for the calculation of cup to disc ratio and ISNT rule calculation. The final decision about the presence of glaucoma is made on the basis of CDR ratio and ISNT notching site. The results of the methods show much better diagnosis than other existing methods.

Chapter 7

Future Directions

Detection and segmentation of optic disc is the wide area of research because of its importance in the detection of other structures such as fovea and macula. The detection of these structures facilitates the development of automated diagnosis systems for DR and AMD. So the accuracy in detection of optic disc results in the accurate and reliable segmentation of disc area which helps the development of CAD for glaucoma, as done in this research work. The implementation of this work has been broken down into the modules as the OD detection, OD segmentation, cup segmentation, and finally glaucoma detection module. This division of modules was done by keeping in mind the extension scenario of this work.

In future, the subparts of this work specially preprocessing, OD detection and segmentation part can be used for development of CAD for DR and AMD. As the proposed methodology in this work is producing accurate detection and segmentation of OD and the percentage of detection is much higher than the other proposed methods in the literature. The detection and segmentation modules have been tested on many publically available databases and comparison of this work in OD detection capability with others available is made in Table 4 while the segmentation performance has been compared in Table 6. To make it more practical for implementing in our country, testing of the method has also been done on local image database from Shifa hospital, Islamabad. As the computer added diagnosis systems have the key importance when it comes to mass screening of population where huge image dataset is required to be processed. Manual detection is not possible, especially in that case. So the complete

system which can diagnose all retinal diseases would be an ideal scenario for the early detection of different diseases to avoid complications of the prolonged disease cases.

References

1. Goldberg, J.L. *Glaucoma and the Brain*. 2016 [cited 2016 17]; Available from: http://www.glaucoma.org/glaucoma/glaucoma-and-the-brain.php.

2. Mittapalli, P.S. and G.B. Kande, *Segmentation of optic disk and optic cup from digital fundus images for the assessment of glaucoma.* Biomedical Signal Processing and Control, 2016. **24**: p. 34-46.

3. Foster, S. *EYE-brary*. [cited 2016 17]; 2016]. Available from: http://www.uveitis.org/patients/support/kids.

4. O'Brien;, K.K. *An Overview of Glaucoma Management for Pharmacists*. 2010 [cited 2016 17]; Available from: https://www.pharmqd.com/node/76880/lesson.

5. *Neuro-ophthalmology*. 2015 [cited 2016 17]; Available from: http://clinicalgate.com/neuro-ophthalmology-2/.

6. *Types of Glaucoma*. 2015 [cited 2016 17]; Available from: http://www.glaucoma.org/glaucoma/types-of-glaucoma.php.

7. Schacknow, P.N. and J.R. Samples, *The glaucoma book: a practical, evidence-based approach to patient care*. 2010: Springer Science & Business Media.

8. Stroud, I. *Tonometry – a preventative procedure for canine glaucoma*. 2012 [cited 2016 17]; Available from: http://www.vet4life.co.uk/tonometry-a-preventative-procedure-for-canine-glaucoma/.

9. Carroll, J.N. *Visual Field Testing: From One Medical Student to Another*. 2013 [cited 2016 17].

10. *Gonioscopy*. 2009 [cited 2016 17]; Available from: https://en.wikipedia.org/wiki/Gonioscopy.

11. *Accutome PachPen Pachymeter*. 2016 [cited 2016 17]; Available from: http://www.keeler.co.uk/accutome-pachpen-pachymeter-406.htm.

REFERENCES

12. *Opthalmoscope*. Available from: http://medical-dictionary.thefreedictionary.com/Monocular+indirect+ophthalmoscopy.

13. *TOPCON TRC-NW200 Fundus Camera*. 2016 [cited 2016 17]; Available from: https://www.dotmed.com/listing/fundus-camera/topcon/trc-nw200/895608.

14. Chaudhuri, S., et al. *Automatic detection of the optic nerve in retinal images*. in *Proceedings of the IEEE International Conference on Image Processing*. 1989.

15. Sinthanayothin, C., et al., *Automated localisation of the optic disc, fovea, and retinal blood vessels from digital colour fundus images.* British Journal of Ophthalmology, 1999. **83**(8): p. 902-910.

16. Lowell, J., et al., *Optic nerve head segmentation.* Medical Imaging, IEEE Transactions on, 2004. **23**(2): p. 256-264.

17. Walter, T. and J.-C. Klein, *Segmentation of color fundus images of the human retina: Detection of the optic disc and the vascular tree using morphological techniques*, in *Medical Data Analysis*. 2001, Springer. p. 282-287.

18. Sekhar, S., W. Al-Nuaimy, and A.K. Nandi. *Automated localisation of retinal optic disk using Hough transform*. in *Biomedical Imaging: From Nano to Macro, 2008. ISBI 2008. 5th IEEE International Symposium on*. 2008. IEEE.

19. Gonzalez, W. and R.E. Woods, *Eddins, 2004, Digital Image Processing Using Matlab*. 2006, Prentice Hall.

20. Rizon, M., et al., *Object detection using circular Hough transform.* 2005.

21. Li, H. and O. Chutatape. *Automatic location of optic disk in retinal images*. in *Image Processing, 2001. Proceedings. 2001 International Conference on*. 2001. IEEE.

22. Osareh, A., et al., *Classification and localisation of diabetic-related eye disease*, in *Computer Vision—ECCV 2002*. 2002, Springer. p. 502-516.

23. Lalonde, M., M. Beaulieu, and L. Gagnon, *Fast and robust optic disc detection using pyramidal decomposition and Hausdorff-based template matching.* Medical Imaging, IEEE Transactions on, 2001. **20**(11): p. 1193-1200.

24. Youssif, A.A.-H.A.-R., A.Z. Ghalwash, and A.A.S.A.-R. Ghoneim, *Optic disc detection from normalized digital fundus images by means of a vessels' direction matched filter.* Medical Imaging, IEEE Transactions on, 2008. **27**(1): p. 11-18.

25. Yu, H., et al. *Fast localization of optic disc and fovea in retinal images for eye disease screening*. in *SPIE Medical Imaging*. 2011. International Society for Optics and Photonics.

26. Hoover, A. and M. Goldbaum, *Locating the optic nerve in a retinal image using the fuzzy convergence of the blood vessels.* Medical Imaging, IEEE Transactions on, 2003. **22**(8): p. 951-958.

27. Foracchia, M., E. Grisan, and A. Ruggeri, *Detection of optic disc in retinal images by means of a geometrical model of vessel structure.* Medical Imaging, IEEE Transactions on, 2004. **23**(10): p. 1189-1195.

28. Ying, H., M. Zhang, and J.-C. Liu. *Fractal-based automatic localization and segmentation of optic disc in retinal images*. in *Engineering in Medicine and Biology Society, 2007. EMBS 2007. 29th Annual International Conference of the IEEE*. 2007. IEEE.

29. Park, J., N.T. Kien, and G. Lee. *Optic disc detection in retinal images using tensor voting and adaptive mean-shift*. in *Intelligent Computer Communication and Processing, 2007 IEEE International Conference on*. 2007. IEEE.

30. Mahfouz, A.E. and A.S. Fahmy, *Fast localization of the optic disc using projection of image features.* Image Processing, IEEE Transactions on, 2010. **19**(12): p. 3285-3289.

31. Roerdink, J.B. and A. Meijster, *The watershed transform: Definitions, algorithms and parallelization strategies.* Fundamenta informaticae, 2000. **41**(1, 2): p. 187-228.

32. Achanta, R., et al., *SLIC superpixels compared to state-of-the-art superpixel methods.* Pattern Analysis and Machine Intelligence, IEEE Transactions on, 2012. **34**(11): p. 2274-2282.

33. Nayak, J., et al., *Automated diagnosis of glaucoma using digital fundus images.* Journal of medical systems, 2009. **33**(5): p. 337-346.

34. Mookiah, M.R.K., et al., *Automated detection of optic disk in retinal fundus images using intuitionistic fuzzy histon segmentation.* Proceedings of the Institution of Mechanical Engineers, Part H: Journal of Engineering in Medicine, 2012: p. 0954411912458740.

REFERENCES

35.   Zhu, X., R.M. Rangayyan, and A.L. Ells, *Detection of the optic nerve head in fundus images of the retina using the hough transform for circles.* Journal of digital imaging, 2010. **23**(3): p. 332-341.

36.   Aquino, A., M.E. Gegúndez-Arias, and D. Marín, *Detecting the optic disc boundary in digital fundus images using morphological, edge detection, and feature extraction techniques.* Medical Imaging, IEEE Transactions on, 2010. **29**(11): p. 1860-1869.

37.   Carmona, E.J., et al., *Identification of the optic nerve head with genetic algorithms.* Artificial Intelligence in Medicine, 2008. **43**(3): p. 243-259.

38.   Köse, C. and C. İkibaş, *Statistical techniques for detection of optic disc and macula and parameters measurement in retinal fundus images.* Journal of Medical and Biological Engineering, 2010. **31**(6): p. 395-404.

39.   Babu, T.G. and S. Shenbagadevi, *Automatic detection of glaucoma using fundus image.* European Journal of Scientific Research, 2011. **59**(1): p. 22-32.

40.   Jonas, J.B., W.M. Budde, and S. Panda-Jonas, *Ophthalmoscopic evaluation of the optic nerve head.* Survey of ophthalmology, 1999. **43**(4): p. 293-320.

41.   McInerney, T. and D. Terzopoulos, *Deformable models in medical image analysis: a survey.* Medical image analysis, 1996. **1**(2): p. 91-108.

42.   Kass, M., A. Witkin, and D. Terzopoulos, *Snakes: Active contour models.* International journal of computer vision, 1988. **1**(4): p. 321-331.

43.   Mendels, F., et al., *Extraction of the optic disk boundary in digital fundus images.* Proceedings BMES/EMBS 1999, 1999. **2**(EPFL-CONF-86620): p. 1139.

44.   Mendels, F., C. Heneghan, and J. Thiran. *Identification of the optic disk boundary in retinal images using active contours*. in *Proceedings of Irish Machine Vision and Image Processing Conference (IMVIP) 1999*. 1999. IEEE.

45.   Xu, C. and J.L. Prince, *Snakes, shapes, and gradient vector flow.* Image Processing, IEEE Transactions on, 1998. **7**(3): p. 359-369.

46.   Osareh, A., et al. *Comparison of colour spaces for optic disc localisation in retinal images*. in *Pattern Recognition, 2002. Proceedings. 16th International Conference on*. 2002. IEEE.

47.   Xu, J., et al., *Optic disk feature extraction via modified deformable model technique for glaucoma analysis.* Pattern recognition, 2007. **40**(7): p. 2063-2076.

REFERENCES

48.   Joshi, G.D., J. Sivaswamy, and S. Krishnadas, *Optic disk and cup segmentation from monocular color retinal images for glaucoma assessment.* Medical Imaging, IEEE Transactions on, 2011. **30**(6): p. 1192-1205.

49.   Ricco, L., *Lipschitz functions*. 2004, Technical report.

50.   Fischler, M.A. and R.C. Bolles, *Random sample consensus: a paradigm for model fitting with applications to image analysis and automated cartography.* Communications of the ACM, 1981. **24**(6): p. 381-395.

51.   Li, H. and O. Chutatape, *Boundary detection of optic disk by a modified ASM method.* Pattern Recognition, 2003. **36**(9): p. 2093-2104.

52.   FENGSHOU, Y., *Extraction of features from fundus images for glaucoma assessment*. 2011, National University of Singapore.

53.   Kim, S.K., et al. *Segmentation of optic nerve head using warping and RANSAC*. in *Engineering in Medicine and Biology Society, 2007. EMBS 2007. 29th Annual International Conference of the IEEE*. 2007. IEEE.

54.   Wong, D., et al. *Level-set based automatic cup-to-disc ratio determination using retinal fundus images in ARGALI*. in *Engineering in Medicine and Biology Society, 2008. EMBS 2008. 30th Annual International Conference of the IEEE*. 2008. IEEE.

55.   Wong, D., et al. *Automated detection of kinks from blood vessels for optic cup segmentation in retinal images*. in *SPIE Medical Imaging*. 2009. International Society for Optics and Photonics.

56.   *DRIVE: Digital Retinal Images for Vessel Extraction*. 2004.

57.   Kauppi, T., et al. *DIARETDB1 diabetic retinopathy database and evaluation protocol*. in *Medical Image Understanding and Analysis (MIUA2007)*. 2007. Aberystwyth, Wales, UK.

58.   Fraz, M.M., et al., *An ensemble classification-based approach applied to retinal blood vessel segmentation.* Biomedical Engineering, IEEE Transactions on, 2012. **59**(9): p. 2538-2548.

59.   Decenciere, E., et al., *Feedback on a publicly distributed image database: the MESSIDOR database.* Image Analysis and Stereology, 2014: p. 231-234.

REFERENCES

60.   Sivaswamy, J., et al., *A Comprehensive Retinal Image Dataset for the Assessment of Glaucoma from the Optic Nerve Head Analysis.* JSM Biomed Imaging Data Pap, 2015. **2**(1): p. 1004.

61.   Fraz, M., et al., *QUARTZ: Quantitative Analysis of Retinal Vessel Topology and size–An automated system for quantification of retinal vessels morphology.* Expert Systems with Applications, 2015. **42**(20): p. 7221-7234.

62.   Abdullah, M. and M.M. Fraz. *Application of grow cut algorithm for localization and extraction of optic disc in retinal images*. in *2015 12th International Conference on High-capacity Optical Networks and Enabling/Emerging Technologies (HONET)*. 2015. IEEE.

63.   Fraz, M.M., et al., *Blood vessel segmentation methodologies in retinal images – A survey.* Computer methods and programs in biomedicine, 2012. **108**(1): p. 407-433.

64.   Fraz, M.M., et al., *Delineation of blood vessels in pediatric retinal images using decision trees-based ensemble classification.* International Journal of Computer Assisted Radiology and Surgery, 2014. **9**(5): p. 795-811.

65.   Foracchia, M., E. Grisan, and A. Ruggeri, *Luminosity and contrast normalization in retinal images.* Medical image analysis, 2005. **9**(3): p. 179-190.

66.   Vázquez, S.G., et al., *Improving retinal artery and vein classification by means of a minimal path approach.* Machine Vision and Applications, 2013. **24**(5): p. 919-930.

67.   Abdullah, M., M.M. Fraz, and S.A. Barman, *Localization and segmentation of optic disc in retinal images using circular Hough transform and grow-cut algorithm.* PeerJ, 2016. **4**: p. e2003.

68.   Fraz, M.M., A. Basit, and S.A. Barman, *Application of Morphological Bit Planes in Retinal Blood Vessel Extraction.* Journal of Digital Imaging, 2012: p. 1-13.

69.   Hough, P.V., *Method and means for recognizing complex patterns*. 1962.

70.   Vezhnevets, V. and V. Konouchine. *GrowCut: Interactive multi-label ND image segmentation by cellular automata*. in *proc. of Graphicon*. 2005. Citeseer.

71.   Toffoli, T. and N. Margolus, *Cellular automata machines: a new environment for modeling*. 1987: MIT Press. 259.

REFERENCES

72.	Fraz, M.M., et al., *Delineation of blood vessels in pediatric retinal images using decision trees-based ensemble classification.* International journal of computer assisted radiology and surgery, 2014. **9**(5): p. 795-811.

73.	Niemeijer, M., M.D. Abràmoff, and B. Van Ginneken, *Fast detection of the optic disc and fovea in color fundus photographs.* Medical image analysis, 2009. **13**(6): p. 859-870.

74.	Welfer, D., et al., *Segmentation of the optic disk in color eye fundus images using an adaptive morphological approach.* Computers in Biology and Medicine, 2010. **40**(2): p. 124-137.

75.	Lu, S., *Accurate and efficient optic disc detection and segmentation by a circular transformation.* Medical Imaging, IEEE Transactions on, 2011. **30**(12): p. 2126-2133.

76.	Zubair, M., A. Yamin, and S.A. Khan. *Automated detection of Optic Disc for the analysis of retina using color fundus image*. in *Imaging Systems and Techniques (IST), 2013 IEEE International Conference on*. 2013. IEEE.

77.	Yu, H., et al., *Fast localization and segmentation of optic disk in retinal images using directional matched filtering and level sets.* Information Technology in Biomedicine, IEEE Transactions on, 2012. **16**(4): p. 644-657.

78.	Saleh, M.D., et al. *Automated segmentation of optic disc in fundus images*. in *Signal Processing & its Applications (CSPA), 2014 IEEE 10th International Colloquium on*. 2014. IEEE.

79.	Yu, T., Y. Ma, and W. Li. *Automatic localization and segmentation of optic disc in fundus image using morphology and level set*. in *Medical Information and Communication Technology (ISMICT), 2015 9th International Symposium on*. 2015. IEEE.

80.	Sopharak, A., et al., *Automatic detection of diabetic retinopathy exudates from non-dilated retinal images using mathematical morphology methods.* Computerized Medical Imaging and Graphics, 2008. **32**(8): p. 720-727.

81.	Walter, T., et al., *A contribution of image processing to the diagnosis of diabetic retinopathy-detection of exudates in color fundus images of the human retina.* Medical Imaging, IEEE Transactions on, 2002. **21**(10): p. 1236-1243.

REFERENCES

82. Seo, J., et al. *Measurement of ocular torsion using digital fundus image*. in *Engineering in Medicine and Biology Society, 2004. IEMBS'04. 26th Annual International Conference of the IEEE*. 2004. IEEE.

83. Kande, G.B., P.V. Subbaiah, and T.S. Savithri. *Segmentation of exudates and optic disk in retinal images*. in *Computer Vision, Graphics & Image Processing, 2008. ICVGIP'08. Sixth Indian Conference on*. 2008. IEEE.

84. Stapor, K., et al., *Segmentation of fundus eye images using methods of mathematical morphology for glaucoma diagnosis*, in *Computational Science-ICCS 2004*. 2004, Springer. p. 41-48.

85. Lupascu, C.A., D. Tegolo, and L.D. Rosa. *Automated detection of optic disc location in retinal images*. in *Computer-Based Medical Systems, 2008. CBMS'08. 21st IEEE International Symposium on*. 2008. IEEE.

86. Welfer, D., J. Scharcanski, and D.R. Marinho, *A morphologic two-stage approach for automated optic disk detection in color eye fundus images.* Pattern Recognition Letters, 2013. **34**(5): p. 476-485.

87. Basit, A. and M.M. Fraz, *Optic disc detection and boundary extraction in retinal images.* Applied Optics, 2015. **54**(11): p. 3440-3447.

88. Morales, S., et al., *Automatic detection of optic disc based on PCA and mathematical morphology.* Medical Imaging, IEEE Transactions on, 2013. **32**(4): p. 786-796.

89. Salazar-Gonzalez, A., et al., *Segmentation of the Blood Vessels and Optic Disk in Retinal Images.* Biomedical and Health Informatics, IEEE Journal of, 2014. **18**(6): p. 1874-1886.

90. Kumar, J.H., A.K. Pediredla, and C.S. Seelamantula. *Active discs for automated optic disc segmentation*. in *2015 IEEE Global Conference on Signal and Information Processing (GlobalSIP)*. 2015. IEEE.